

1998

Velocity profile in confined elliptic fractures

Stephen Ronald Pack Jr.
West Virginia University

Follow this and additional works at: <https://researchrepository.wvu.edu/etd>

Recommended Citation

Pack, Stephen Ronald Jr., "Velocity profile in confined elliptic fractures" (1998). *Graduate Theses, Dissertations, and Problem Reports*. 931.
<https://researchrepository.wvu.edu/etd/931>

This Thesis is protected by copyright and/or related rights. It has been brought to you by the The Research Repository @ WVU with permission from the rights-holder(s). You are free to use this Thesis in any way that is permitted by the copyright and related rights legislation that applies to your use. For other uses you must obtain permission from the rights-holder(s) directly, unless additional rights are indicated by a Creative Commons license in the record and/ or on the work itself. This Thesis has been accepted for inclusion in WVU Graduate Theses, Dissertations, and Problem Reports collection by an authorized administrator of The Research Repository @ WVU. For more information, please contact researchrepository@mail.wvu.edu.

VELOCITY PROFILE IN CONFINED ELLIPTIC FRACTURES

By

Stephen Ronald Pack, Jr.

A Thesis

Submitted to
The College of Engineering
at
West Virginia University

In Partial Fulfillment of the Requirements
For the Degree of

Master of Science
in
Mechanical Engineering

Department of Mechanical and Aerospace Engineering

Morgantown, West Virginia
December 1998

ABSTRACT

VELOCITY PROFILE IN CONFINED ELLIPTIC FRACTURES

Stephen Ronald Pack, Jr.

Predicting the effect of friction on fluid flow inside a hydraulically induced fracture is an important problem in the design of successful oil and natural gas fracture treatments of wells. Hydraulic fracturing is the process of using hydraulic pressure to create a fracture in an oil or gas bearing formation and distribute propping agents along the fracture to hold it open after the treatment is completed. The primary objective of this research is to determine the friction inside a smooth fracture. Also incorporate the effect of friction on a fluid transient inside a tapered-elliptical-confined fracture. In order to do so, the non-uniform velocity profile in an elliptic fracture with laminar flow of both Newtonian and non-Newtonian fluids was calculated. A transient flow computer program is presented using the method of characteristics, to show the frictional effects on acoustic damping. The pressure pulse of an acoustic wave reflection, caused by a fluid transient during fracturing, is proportional to the steady state velocity and density of the fluid. The pressure pulse considered here is caused by a sudden fractional change in mass flow rate. For one-dimensional flow its magnitude is $\Delta p = -\rho c \Delta V = -rc \frac{\Delta q}{A}$, where ρ is the fluid density, c is the wave speed and ΔV is the change in fluid velocity. In tubing with turbulent flow, the velocity profile is fairly flat, thus approximately equal to V_{av} . Note Δq is the change in volume flow rate. However for flow inside a hydraulic fracture, the 3D velocity profile is highly non-uniform, and the use of V_{av} creates an error as $V_{max} \gg V_{av}$. The variation in hydraulic diameter associated with an elliptic

cross-section of a confined fracture as given by the Perkins/Kern model⁶ is responsible for the large difference between V_{\max} and V_{av} . It is shown that for a smooth wall, elliptic fracture, with laminar Newtonian flow, $V_{\max} = 2.66 V_{\text{av}}$.

ACKNOWLEDGEMENTS

I would like to thank Jesus Christ for blessing me with the engineering talent and persistence needed to complete my thesis and education. My sincere appreciation to my research advisor and committee chairman, Dr. John Loth, for his guidance and teaching throughout the course of my research at West Virginia University. I would also like to thank my committee members, Dr. Ken Means and Dr. Scott Wayne. I would like to thank Jeremy King for his constant input and assistance throughout my research effort. I wish to thank Jennifer Hoppie for her editing and continual support and encouragement. I wish to acknowledge Richard Guiler for his contribution on this research project. To all the friends that I have met here at West Virginia University, thank you.

The Halliburton Company sponsored funding for this project.

Finally, very special thanks to my parents, Steve and Rita Pack, for the love and encouragement that they showed me throughout my education and life.

TABLE OF CONTENTS

TITLE PAGE.....	i
ABSTRACT.....	ii
ACKNOWLEDGEMENTS.....	iv
TABLE OF CONTENTS.....	v
LIST OF TABLES.....	vii
LIST OF FIGURES.....	viii
NOMENCLATURE.....	ix
CHAPTER 1-INTRODUCTION.....	1
1.1 Introduction.....	1
1.2 Fracturing Effects.....	1
1.3 Acoustic Well Characteristics.....	4
1.4 Method of Characteristics.....	5
1.5 Research Objective.....	11
CHAPTER 2-LITERATURE REVIEW.....	14
2.1 Hydraulic Fracturing Theory.....	14
2.2 Predicting Fracture Width.....	16
2.3 Methods to Determine Fracture Height.....	18
2.4 Rock Mechanics.....	20
2.5 Basic Relations.....	23
2.6 In-Situ Stress.....	25
2.7 Effect of In-Situ Stresses and Rock Properties on Geometry.....	27
2.8 Fluid Loss From Hydraulically Induced Fractures.....	32

CHAPTER 3-VELOCITY PROFILE MODELING.....	34
3.1 Steady 2D Laminar Flow Model for an Elliptic Fracture.....	34
3.2 Model Boundary Conditions.....	34
3.3 Pressure Gradient Derivation.....	36
3.4 Errors Associated With Assuming V_{av} Across Fracture.....	42
CHAPTER 4-ACOUSTIC WELL CHARACTERISTICS ANALYSIS.....	44
4.1 Acoustic Analysis	44
4.2 Procedure.....	45
4.3 Steady Flow Boundary Conditions.....	46
4.4 Transient Flow Boundary Conditions.....	46
4.5 Well Tube Casing and Fracture Data.....	47
CHAPTER 5-RESULTS AND DISCUSSION.....	49
5.1 Steady State Results	49
5.2 Transient Flow Results.....	50
5.3 Figure Results and Explanation.....	51
CHAPTER 6-CONCLUSIONS AND RECOMMENDATIONS.....	55
6.1 Conclusion.....	55
6.2 Recommendations for Future Study.....	56
REFERENCES.....	57
APPENDIX A.....	59
APPENDIX B.....	72
VITA.....	77
APPROVAL OF EXAMINING COMMITTEE.....	78

LIST OF TABLES

	Title	Page Number
1.1	Comparison of Final Fracture Dimensions with 2D Values	2
3.1	Comparison of Measured vs. Theoretical Friction Factors in a Hydraulic Fracture	38
4.1	Tube Data	47
4.2	Fracture Data	48
5.1	Steady State Tube Data	49
5.2	Steady State Fracture Data	50
5.3	Transient Flow Calculations for the Well Tube	50
5.4	Transient Flow Calculations for End Tube Station and Fracture	51

LIST OF FIGURES

	Title	Page Number
1.1	Examples with the Different Characteristic Slopes	3
1.2	Characteristic Lines in the x-t Plane	8
1.3	x-t Grid for Solving Single-Pipe Problems	9
2.1	In-situ Stress Below Interface	30
3.1	3D Velocity Profiles Caused by Friction	39
3.2	Measured and Simulated Net Pressure: Opening Natural Fissures	42
5.1	H1,1 vs. Time	53
5.2	H2,1 vs. Time With Fracture Friction = $\frac{64}{N Re}$	53
5.3	H2,1 vs. Time With Fracture Friction = 0.0028	54
5.4	Fluid Flow Rate vs. Time	54

NOMENCLATURE

a_1	Width of near-crack-tip zone (ft)
A	Tube area
A_x	Fracture cross-sectional area varying with x
c	Wave propagation velocity (ft/sec)
D_H	Hydraulic diameter
E	Young's modulus
E'	The effective Young's modulus due to the overburden pressure
f	Friction coefficient
fD	Darcy friction coefficient
FE	Fluid efficiency
G	Pad fluid gel
H	Hydraulic head
h	Fracture height
L_f	Length of the fracture
L_{fav}	Length of fracture based on average velocity
N	Number of reaches in tube or fracture
NRe	Reynolds number for Newtonian fluid
NRe'	Reynolds number for power law fluid
n' and K'	Power law coefficients
p	Fluid pressure
p_{is}	Instantaneous shut in fluid pressure
p_{Lf}	Fluid pressure at end of fracture
$Prop$	Fluid proppant content
q	Fluid flow rate (ft ³ /s)
q_f	Fluid flow rate entering a single fracture
q_p	Fluid pumping rate into well tube
r_t	$f_{\text{experimental}}/f_{\text{lam}}$
RMS	Root mean square
t	Time
V	Velocity
V_{av}	q/A_x the average velocity
V_{max}	Maximum centerline velocity varies with x
$V_{m,x}$	Centerline velocity averaged over y direction with assumed parabolic Pousseulle flow velocity profile
$V_{z,x}$	Fracture velocity at any distance z from centerline but averaged over y direction with assumed parabolic Pousseulle flow velocity profile
Vol_p	Volume of fluid pumped
Vol_f	Volume of the fracture
w	Fracture width, with subscript (av) means average
$w_{m,o}$	Centerline width at origin of fracture
$w_{m,x}$	Centerline width of fracture
$w_{z,x}$	Width of fracture at any distance z from centerline
x	Fracture centerline axis measured from well casing
σ	Drag ratio correction factor defined by Lord/McGowan

σ_{\min}	Minimum in-situ stress or fracture closure stress
σ_c	Confining stress
ϕ	Porosity of the surface
ν	Poisson's ratio
ε	Relative roughness inside fracture
ρ	Fluid density
μ	Fluid viscosity
τ	Acoustic wave period, subscript (t) for tube and (f) for fracture

CHAPTER 1

INTRODUCTION

1.1 Introduction

The demand for oil and natural gas has remained stable over the years. In about 50% of the wells, applying hydraulic rock fracturing can increase production. Hydraulic rock fracturing consists of pumping fluid at a high volume rate and increasing pressure into the perforated well casing. Various aspects of this process have been reviewed in chapter 2.

1.2 Fracturing Effects

Hydraulic fracturing is basically the creation of artificial flow channels in rock. These flow channels are intended to increase reservoir production. The geology of the rock where fracturing occurs must also be considered. When stimulating a well, the fracturing pressure must be carefully controlled to avoid fracturing through the confining layers into a water-carrying vein.

Many, so-called 2D and 3D closed form solutions, have been developed in the 1960's. Each based on different simplifying assumptions to deal with the complex solid-fluid mechanics interaction problem. The various models result in different fracture length predictions as shown in Table 1.1.

Table 1.1 Comparison of Final Fracture Dimensions with 2D Values from Reference 1

Model	Total Fracture Length (ft)	Maximum Wellbore Width (ft)
3D	1800	0.224
PKN simplified model	2305	0.212
GdK simplified model	1882	0.239
PKN computer model	2400	0.195
KZ computer model	1416	0.280

With change in fracture length there is a corresponding difference in the bottom hole pressure-time history. The model that closest resembles the actually measured pressures is likely to be the one preferred by the fracturing supervisor. Nolte and Smith² discuss four pressure-time histories, each exhibiting a different pressure-time exponent during fracturing. The modes are: Mode I with small positive slope (this mode is the most common); Mode II with zero slope or at constant pressure (associated with either a sudden increase in fluid loss, height or compliance); Mode III with unit slope (e.g. proppant screenout); Mode IV with negative slope (associated with rapid height growth). Mode I represents a fracture propagating under the assumption for slope bounds of 0.125→0.25. This is the most common as well as the most desired type of fracturing. Mode II has constant pressure, which is likely caused by fluid leakage equal to input fluid, which leads to constant width and thus pressure. Mode III indicates that proppant causes a barrier, which prevents further length growth. Then the fracture width must grow to accommodate the entering fluid. This time linear growth in width is directly proportional to the rate of pressure build up. Mode IV depicts that the fracture

is propagating outwardly and upwardly into the confinement layers. Propagating into confinement layers could lead into fracturing into a water reservoir and flooding out the well. Obviously it is very difficult to incorporate these various Modes of operation in one theoretical model.

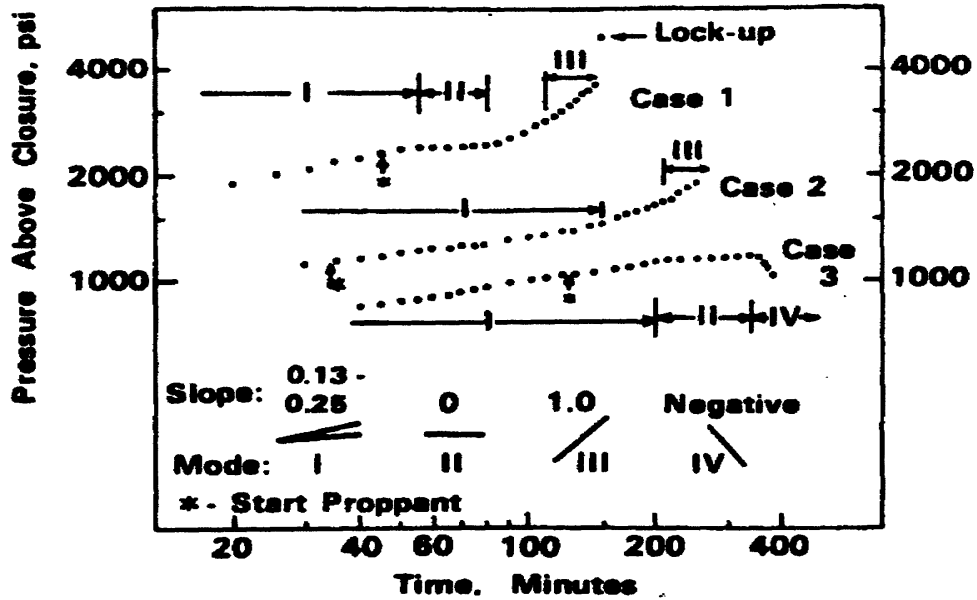


Figure 1.1
Examples with the Different Characteristic Slopes from Reference 2

The solution obtained depends on the boundary conditions imposed. An important aspect is the fluid efficiency (FE), which is a measure of the fluid available for fracture volume creation. As a result, the volume of fluid pumped (Vol_p), when multiplied by FE gives the volume of the fracture (Vol_f). The loss of fluid into the rock is given by Darcy's law and is a function of time. The pumping flow rate (q) needs to be maximized in order to maximize FE.

1.3 Acoustic Well Characteristics

During the rock fracturing process the length, L , of a confined fracture is estimated from the fracture volume, the confining fracture height, h , and the average width, w . The fluid volume in the fracture is equal to the volume of fluid pumped minus fluid loss into the formation and the average width is calculated from measured fluid pressure and minimum in-situ stress. Then, $L = (\frac{1}{2} \text{ fluid volume}) / (w * h)$. Due to the approximations associated with this calculation of fracture length, another technique was being pursued. This method was based on measuring the natural frequency of pressure oscillations inside the fracture. The natural frequency is inversely proportional to fracture length as given by: $\text{frequency} = c / 4L$.

It is possible to calculate the fracture wave oscillation natural frequency, when the pressure pulses, generated by either natural or imposed fluid transients, become identifiable. These pressure pulses are proportional to the flow velocity inside the fracture and inversely proportional to viscous damping and fluid leakage. Non-Newtonian gel fluids are used to reduce friction and to create a filter cake, which eliminates fluid losses through the fracture wall into the formation. Caking is the process of filling cracks and valley's in the rock surface with long chain molecules. The result is that fluid leakage, defining fluid efficiency, is restricted to the region near the newly formed fracture. This is important for the assumption that the fluid pumped multiplied by the fluid efficiency, equals the volume growth rate in two opposing fractures.

1.4 Method of Characteristics

To investigate the acoustic well characteristics during hydraulic rock fracturing, a one-dimensional method of characteristics was applied to a well with a defined geometry and two opposing confined fractures. The method of characteristics has been fully described by Chaudry³ and Wylie⁴. It is a time-step marching solution of the continuity and momentum equations. The continuity and momentum equations are different from those found in most fluids text books because some terms can be neglected in fluid transients and other terms are added to account for the expansion of the pipe, at the high pressure changes. From Newton's second law of motion the momentum equation is derived:

$$dF = dm * dV/dt$$

The friction shear force acting on an element of fluid inside a differential length of pipe, of diameter D is given by the Darcy-Weisbach formula.⁴

$$dF_f = (f/4) \frac{1}{2} \rho V^2 \pi D dx$$

The differential pressure force is given by

$$dF_p = -A \frac{\partial p}{\partial x} dx = -r g A \frac{\partial H}{\partial x} dx$$

Differential mass, $dm = \rho A dx$ and acceleration, $\frac{dV}{dt} = \frac{\partial V}{\partial t} + V \frac{\partial V}{\partial x}$ inserted above

$$\text{gives: } -r g A \frac{\partial H}{\partial x} + \left(\frac{f}{4}\right) \frac{1}{2} r A V^2 \left(\frac{4}{D}\right) = r A \left(\frac{\partial V}{\partial t} + V \frac{\partial V}{\partial x}\right).$$

To account for reverse flow use: $V^2 = V|V|$ and neglect the term $V \frac{\partial V}{\partial x}$ as it is small

relative to $\frac{\partial V}{\partial t}$ in transient flow. The momentum equation in reference 4 becomes

$$g \frac{\partial H}{\partial x} + \frac{\partial V}{\partial t} + \frac{fV|V|}{2D} = 0. \quad (1-1)$$

The continuity equation equates the change in volume, $dVol$, under the applied wave pressure due to change in volume from fluid compressibility and that from pipe expansion or contraction.

If the bulk modulus of elasticity of the fluid is defined by $K = -Vol \frac{dp}{dVol}$,

then the change in volume due to fluid compressibility is

$$dVol = -\frac{dpAdx}{K} = -\frac{\partial p}{\partial t} \frac{Adxdt}{K}. \text{ The change in pipe volume due to the increase in}$$

radius $dVol = 2\pi r drdx$. When the wall thickness is (e) and the wall material modulus of elasticity is (E) , then the change in pressure causes a circumferential stress (σ)

related to strain, or $s = E \frac{dr}{r}$. The pressure rise is related to the increase in

circumferential stress $s = \left(\frac{r}{e}\right) dp$ or $\frac{rdp}{e} = E \frac{dr}{r}$. Solving for $dr = dp \frac{r^2}{eE}$

$$dVol = 2\pi \frac{r^3}{eE} dpdx = \frac{AD}{eE} \frac{\partial p}{\partial t} dxdt. \text{ Equating the increase in pipe volume to the}$$

change in fluid volume plus the net volume in flow of fluid into control volume, Adx ,

in time dt gives $\frac{AD}{eE} \frac{\partial p}{\partial t} dxdt = -\frac{\partial p}{\partial t} \frac{Adxdt}{K} - A \frac{\partial V}{\partial x} dxdt$. Defining the square of the

wave speed inside the fluid by: $c^2 = \frac{1}{r\left(\frac{1}{K} + \frac{D}{eE}\right)}$ gives $\frac{\partial V}{\partial x} + \frac{\partial p}{\partial t} \left(\frac{1}{pc^2}\right) = 0$, or in

terms of fluid head $H = \frac{p}{rg}$ gives continuity equation in reference 4:

$$\frac{c^2}{g} \frac{\partial V}{\partial x} + \frac{\partial H}{\partial t} = 0 \quad (1-2)$$

where

A = pipe area

c = speed of sound

D = pipe diameter

f = Darcy's friction factor

g = acceleration of gravity

H = hydraulic head

p = pressure

V = velocity

Vol = volume

dx = element of pipe length

dt = time step

ρ = fluid density

σ = circumferential stress increase

These two partial differential equations can be converted to ordinary differential equations by the method of characteristics and are only valid along specific directions as given by the C^+ and the C^- equations. Integrating the resulting ordinary differential equations can be done by either graphical or numerical means in the x-t plane. They are grouped and identified as the C^+ and C^- equations. This is explained in detail in reference 4, with a portion duplicated here in single spacing in the remainder of this Section 1.4.

$$C^+ : \begin{cases} \frac{g}{c} \frac{dH}{dt} + \frac{dV}{dt} + \frac{fV|V|}{2D} = 0 & (1-3) \\ \frac{dx}{dt} = +c & (1-4) \end{cases}$$

$$C^- : \begin{cases} -\frac{g}{c} \frac{dH}{dt} + \frac{dV}{dt} + \frac{fV|V|}{2D} = 0 & (1-5) \\ \frac{dx}{dt} = -c & (1-6) \end{cases}$$

Thus the two partial differential equations have been converted to two total differential equations, Eqs. (1-3) and (1-5), each with the restriction that it is valid only when the respective Eqs. (1-4) and (1-6) are valid.

It is convenient to visualize the solution as it develops on the independent variable plane (i.e. the x-t plane). Inasmuch as c is generally constant for a given pipe, Eq. (1-4) plots as a straight line on the x-t plane; and similarly Eq. (1-6) plots as a different straight line. This is shown in Figure 1.2 below. These lines on the x-t plane are the characteristic lines along which Eqs. (1-3) and (1-5) are valid. The latter equations are referred to as compatibility equations, each one being valid only on the appropriate characteristic line. No mathematical approximations have been made in this transformation of the original partial differential equations. Thus every solution of this set will be a solution of the original system given by Eqs. (1-1) and (1-2).

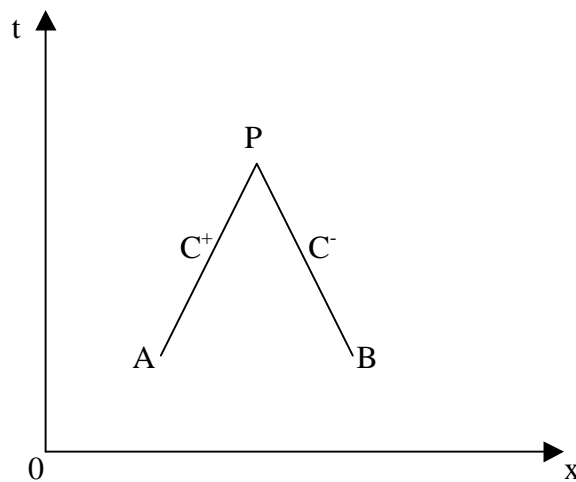


Figure 1.2
Characteristic Lines in the x-t Plane from Reference 4

A pipeline is divided into an even number of reaches, N , each Δx in length, as shown in Figure 1.3 below. A time-step size is computed, $\Delta t = \Delta x/c$, and Eq. (1-4) is satisfied by a positively sloped diagonal of the grid, shown by the line AP . Since N is an even integer the time step is also an even submultiple of the transit time, L/c . If the dependent variables V and H are known at A , then Eq. (1-3), which is valid along the C^+ line, can be integrated between the limits A and P , and thereby be written in terms of unknown variables V and H at point P . A negatively sloped diagonal of the grid, shown by BP satisfies Eq. (1-6). Integration of the C^- compatibility equation along the line BP , with conditions known at B and unknown at P , leads to a second equation in terms of the same two unknown variables at P . A simultaneous solution yields conditions at the particular time and position in the x - t plane designated by point P .

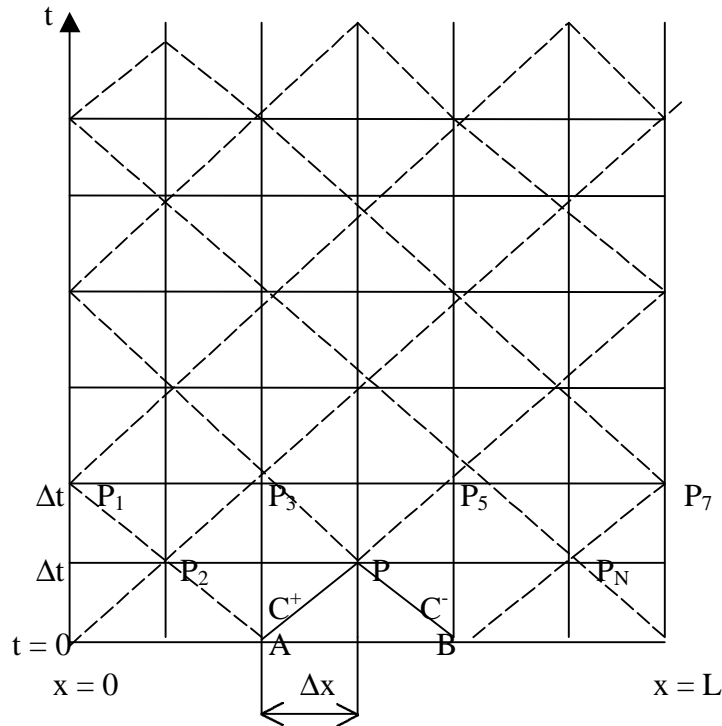


Figure 1.3
x-t Grid for Solving Single-Pipe Problems from Reference 4

By multiplying Eq. (1-3) by $\frac{cdt}{g} = \frac{dx}{g}$, and by introducing the pipeline area to write the equation in terms of discharge in place of velocity, the equation may be placed in a form suitable for integration along the C^+ characteristic as shown in Figure 1.3.

$$\int_{H_A}^{H_P} dH + \frac{c}{gA} \int_{Q_A}^{Q_P} dQ + \frac{f}{2gD_H A^2} \int_{x_A}^{x_P} Q |Q| dx \quad (1-7)$$

The variation of Q with x under the integral in the last term is unknown, thus an approximation must be introduced in this evaluation. The trapezoidal rule was used in this evaluation. It is of second-order accuracy, maintains the linear form of the integrated equations, and is a satisfactory approximation for most problems. The integration of along the C⁻ characteristic between B and P yields

$$H_P - H_A + \frac{c}{gA} (Q_P - Q_A) + \frac{f\Delta x}{2gDA^2} Q_P |Q_A| = 0 \quad (1-8)$$

$$H_P - H_B - \frac{c}{gA} (Q_P - Q_B) - \frac{f\Delta x}{2gDA^2} Q_P |Q_B| = 0 \quad (1-9)$$

These two compatibility equations are basic algebraic relations that describe the transient propagation of piezometric head and flow in a pipeline. By solving for H_P, these equations may be written

$$C^+ : \quad H_P = H_A - B(Q_P - Q_A) - RQ_P |Q_A| \quad (1-10)$$

$$C^- : \quad H_P = H_B + B(Q_P - Q_B) + RQ_P |Q_B| \quad (1-11)$$

in which B is a function of the physical properties of the fluid and the pipeline, often called the pipeline characteristic impedance:

$$B = \frac{c}{gA} \quad (1-12)$$

and R is the pipeline resistance coefficient:

$$R = \frac{f\Delta x}{2gD_H A^2}. \quad (1-13)$$

The friction factor, f, may be a constant, or it may be adjusted with the local Reynolds number in accordance with the Moody diagram in each reach at each time step during calculations.

These equations satisfy steady conditions in the pipe since the flows are equal, $Q_A = Q_P = Q_B$ and $RQ_P |Q_A|$ is the steady-state friction head loss over the reach Δx . If an exponential friction formula is preferred, the last term of Eq. (1-10), for example, would become $R'Q_P |Q_A|^{n-1}$, with n the exponent in the friction loss equation and R' is the coefficient.

The solution to a problem in liquid transients usually begins with steady-state conditions at time zero, so that H and Q are known initial values at each computing section (Fig. 1.3), for $t = 0$. The solution consists of finding H and Q for alternate grid points along $t = \Delta t$, then proceeding to $t = 2\Delta t$, and so on, until the desired time duration has been covered. At any interior grid intersection point, point P at section i,

the two compatibility equations are solved simultaneously for the unknowns Q_i and H_i . Equations (1-10) and (1-11) may be written in a simple form, namely

$$C^+ : H_i = C_P - B_P Q_i \quad (1-14)$$

$$C^- : H_i = C_M + B_M Q_i \quad (1-15)$$

in which the coefficients C_P , B_P , C_M , and B_M are known constants when the equations are applied. Their values in the C^+ and C^- compatibility equations are, respectively :

$$C_P = H_{i-1} + B Q_{i-1} \quad B_P = B + R|Q_{i-1}| \quad (1-16)$$

$$C_M = H_{i+1} - B Q_{i+1} \quad B_M = B + R|Q_{i+1}| \quad (1-17)$$

By first eliminating Q_i in Eqs (1-14) and (1-15), we have

$$H_i = \frac{C_P B_M + C_M B_P}{B_P + B_M} \quad (1-18)$$

Then Q_i may be found directly from either Eq. (1-14) or (1-15) or from

$$Q_i = \frac{C_P - C_M}{B_P + B_M} \quad (1-19)$$

The subscript notation used in the equations above, which is convenient for computer calculations, is shown in Fig. 1.3. It may be noted that section i refers to any grid intersection point in the x direction. Subscripted values of H and Q at each section are always available for the preceding time step, either as given initial conditions or as the result of a previous stage of the calculations.

Numerical values of H and Q are found at alternate grid intersection points P_2 , P , and P_N (Fig. 1.3) at time $1\Delta t$; then time is incremented by Δt and the procedure is repeated for interior grid intersection points P_3 and P_5 (Fig. 1.3) at time $2\Delta t$. Examination of the grid in Fig. 1.3 shows that the endpoints of the system are introduced every other time step after the initial conditions. Therefore, to complete the solution to any desired time, it is necessary to introduce appropriate end conditions, called boundary conditions.⁴

1.5 Research Objective

A one-dimensional transient flow solution using the method of characteristics is presented in this research work. It demonstrates the acoustic response based on an average velocity inside the fracture, assuming it behaves like a one-dimensional tube.

As the transient induced pressure pulses are directly proportional to velocity inside the tube, the primary objective of this research was to determine how the maximum velocity inside the fracture differs from the average velocity $V_{av} = q/A$ which is used in the transient flow computer program. This investigation was limited to fluid flow inside smooth wall fractures with both Newtonian and non-Newtonian gel fluids. Newtonian fluids are fluids such as water, air, and gasoline. If a fluid is Newtonian then the shear stress acts on a plane normal to the y-axis, $t_{yx} \propto \frac{dV}{dy}$. The term non-Newtonian classifies fluids in which shear stress is not directly proportional to deformation rate. Thus they are said to be time-dependent or time-independent. They may be adequately represented by the power law model, which for one-dimensional flow becomes $t_{yx} = k \left(\frac{dV}{dy} \right)^n$. The surface roughness, RMS or root mean square, has not been considered in this analysis for smooth surface fractures. In reality the surface roughness may be assumed to disappear when using gel fluids, which cover the fracture with a filter cake of thickness RMS. The resulting flow area loss to the fracture area $A = h \cdot w_{av}$ is given by $A_{loss} = 2RMS \cdot h$. Thus, caking increases all fluid velocities by the ratio $\frac{A}{A - A_{loss}} = \frac{w_{av}}{w_{av} - 2RMS}$.

In an effort to define the research project, various aspects of hydraulic fracturing and fracture geometry were studied. A review of some relevant papers on the subject has been presented in Chapter 2. It became apparent that more work needs to be done in the area of predicting fluid friction loss inside the fracture. Friction loss is a function of fluid types, fracture geometry, surface roughness, and

flow rate. This is dealt with in detail in later chapters. The actual velocity profile was compared with the average velocity in order to bring in perspective the validity of using V_{av} in the transient flow analysis program. Chapter 3 gives the equation derivations for the actual velocity profile compared to the average velocity for Newtonian flows. The more complex non-Newtonian flows are covered in Appendix A. Chapter 4 shows the results using the average velocity in the transient flow analysis program.

Chapter 2

Literature Review

2.1 Hydraulic Fracturing Theory

The first rock fracturing techniques were developed in 1948. These techniques were commercialized a year later, leading to lofty praise due to their high success ratio. Within a few years, thousands of wells per year were being stimulated by hydraulic fracturing techniques.⁵

Hydraulic fracturing techniques were created in order to increase production of wells. Oil and natural gas accumulate in the pores and natural spaces of subsurface rocks. A permeable rock has interconnected pores. These interconnections form channels through which the oil or natural gas can flow. Low permeability describes rock whose channels are small, restricting fluid flow. High permeability describes rock whose channels allow fluid to flow easily. Both types of rock present problems in the commercial market of extracting oils and natural gas. In high permeable rock, drilling fluid may enter the flow channels leading to the blockage of these channels; therefore, restricting fluid flow in the production phase. In low permeable rock, the channels may be too restrictive to allow the fluid to flow into the wellbore. Often it is beneficial to create artificial channels in the rock to increase fluid flow into the wellbore.

During hydraulic fracturing, fluid fills the wellbore under pressure applied at the surface. The pressure of the fluid in the rock pores also increases. This hydraulic pressure is applied equally in all directions. When the fluid pressure exceeds the minimum in-situ compression stress, the rock will part, as its tensile strength is negligible. Any additional pressure causes the rock walls to elastically compress. The

fracture length will extend as long as sufficient pressure is maintained by injection of additional fluids. To prevent closure in these fractures, propping agents are often placed inside the fracture. A propping agent is a material that has high permeability in proportion to the surrounding formation. It is strong enough to hold the fracture open after the fracturing process is completed. This creates better production phase flow, through the fracture, into the well bore.

Proppant concentration is an important part of the hydraulic fracturing process. There are two proppant concentrations to be considered: (the concentration at the surface in pounds per gallon at the pumps) and (the concentration in the fracture in pounds per square foot of fracture surface area).⁶ It must be noted that the proppant concentration at the pump is evaluated differently when using a conventional fluid rather than a viscous fluid.

Conventional fracturing fluid allows the proppant to settle and pack the bottom of the fracture. Published equations have indicated that the fracture width is dependent upon the viscosity of the fracturing fluid, injection rate, and fracture length. The advantage of using high proppant concentrations with conventional fracturing fluids is to increase the proppant bed height.

Due to advancements in technology, high viscosity fracturing fluids are now available. These highly viscous fluids are known as proppant-suspending fluids. Proppant-suspending fluids make it possible to transport proppant greater distances from the wellbore as well as being able to prop the created fracture over its entire height. In proppant-suspending fluids, the proppant concentration is not directly dependent upon the fracture width, as was the case with conventional fluids. Yet, the

fracture width still affects the size and concentration of the proppant that may be placed in the fracture.

Calculating the concentration of the proppant in a fracture for a proppant-suspending fluid may be done only if the surface area of the fracture is known. Also, only an average concentration of proppant in the fracture can be calculated unless the proppant is started at a specific concentration at the pump and is held constant throughout treatment.

The advantages of using a proppant-suspending fluid over a conventional fluid with the same proppant concentration, is that proppant is distributed over greater lengths and heights. When using a conventional fluid, it could lead to low proppant concentration throughout the fracture. Studies have determined that low proppant concentration in the fracture may cause extensive crushing and low fracture flow capabilities.

2.2 Predicting Fracture Width

Predicting fracture width and length is a common problem in the oil and natural gas industry today. The prediction of these variables would allow for more efficient design of the fracture treatment and increased well productivity. During the hydraulic fracturing treatment of an oil or gas well, the liquid pressure in the borehole is increased until the tensile stress in the surrounding rock exceeds its tensile strength.⁷ The rock will fracture along the path of least resistance which, is the path of least compressive stress. Yet, it remains uncertain whether the values chosen for the operational parameters, such as injection rate, pumping time and fluid viscosity,

are in fact the ideal ones.⁷ From past experience, there is a significant databank to make rough predictions; however, a more thorough method is desired to analyze the fracturing propagation process. Such a method should maximize the use of measurable parameters, allowing the field engineer to more accurately predict the fracture results.

The study of fluid mechanics, material mechanics, and the theory of elastic deformation of rocks, shows that the fluid pressure drop in the fracture controls the width of a hydraulically induced fracture. The operating conditions that cause high-pressure drop along the crack, i.e. high pumping rate and viscous fluids, will result in a relatively wide fracture. Operating conditions, which cause low-pressure drop, i.e. low pumping rate and non-viscous fluids, will result in a relatively narrow fracture.⁸ Understanding the width growth of fractures during the creation of the fracture is very important. Knowing this information would allow for fracture volume predictions to be made under varied conditions. Under moderate stress conditions like the conditions that are usually encountered during hydraulic fracturing, and when more stress is rapidly applied, most rocks fail in a brittle manner.⁸ Therefore the assumption has been made that rocks behave as an elastic and brittle material.

Fractures in the vertical direction can sometimes be limited by conditions of the earth. In limestone reservoirs, nonpermeable section may have higher horizontal stresses than permeable sections after the reservoir pressure has been drawn down.⁸ The fracture will continue to grow vertically until it reaches such a zone. Once this zone is reached the fracture will then continue to grow laterally outward from the wellbore. The fracture penetrates up and down into the bounding zones until

equilibrium is reached. If the bounding zones are not thick enough or if the pressure drop inside the fracture becomes too high, then the fracture may crack through into other zones. This may result in the loss of oil or natural gas into these zones during extraction.

2.3 Methods to Determine Fracture Height

Temperature surveys are generally the most reliable method for estimating fracture height at the wellbore. There are times when these surveys may be inconclusive, but in general they are the most reliable method. These methods included (1) laboratory and field measurements of thermal conductivity, (2) computer simulation of temperature surveys, (3) postfracture gamma ray logs to locate radioactive proppant, (4) radial differential temperature (RDT) log, and (5) noise log. In the oil and gas industry, massive hydraulic fracturing (MHF) has become vital. Formations with microdarcy permeability can now be created because of MHF treatments.⁹

In theory the incorporation of temperature logs can be used to estimate wellbore fracture height. Temperature logs have been used for years to estimate the wellbore fracture height created by hydraulic fracturing. Agnew in 1965 presented the theory and the interpretation method of postfracture temperature surveys.⁹ His method remains the most reliable method to determine fracture height. The drawback of his method is that surveys are sometimes difficult to interpret. Difficulties arise due to unusual temperature behavior adjacent to the treatment zone.

One of the unusual temperature behavior patterns on a postfracture survey is a warm anomaly of 10 to 80°F (-12 to 26°C) above the treatment zone.⁹ This anomaly has the potential to extend several hundred feet above the intended zone. To understand the postfracture temperature surveys, two basic approaches were used. First, laboratory measurements, computer simulations, and prefracture temperature surveys were used to study the effects of thermal conductivity variation. Second, three production logging techniques were used to substantiate the interpretation of temperature logs.⁹ To detect radioactive proppant, the logs were used with postfracture gamma ray log, RDT, and the noise log. The results from these methods allow a better understanding and estimation of fracture height from temperature surveys. It should be noted that all methods currently available for measuring fracture height have a small radius of investigation. This radius is about 2 feet.

To interpret post fracture temperature surveys correctly, the thermal conductivity variations in the earth must be considered. Depending upon the mineral content of the rock, the thermal conductivity may change. The thermal conductivity affects the geothermal gradient in a wellbore. Yet, there is little known on how thermal conductivity affects the postfracture temperature surveys. It is known that the temperature measured by postfracture temperature surveys is related inversely to the rock thermal conductivities.⁹ Rocks with high thermal conductivity tend to change temperature at a slower rate than rocks with low thermal conductivity. Thus, when a cool fluid is pumped into a hot wellbore, the zones that are of high thermal conductivity cool less than the zones of low thermal conductivity. Knowing the thermal conductivity characteristics of a formation allows the location of anomalies

on postfracture surveys to be predicted. After identifying the anomalies caused by conductivity changes, it is possible to determine which anomalies are caused by fractures.

2.4 Rock Mechanics

When performing hydraulic fracturing, the mechanical properties of the rock must be considered. Rock mechanics is important in the determination of these basic mechanical properties as well as the in-situ stresses in the rock. In order to predict minimum fracture extension pressures, the physical properties of the rock must be determined. The mechanical properties that are usually considered for a treatment design are (1) elastic properties, which include the elastic modulus (E), the modulus of rigidity or shear modulus (G), and Poisson's ratio (ν); (2) strength properties such as material tensile and compressive strength as well as fracture toughness; (3) the ductility of the material; (4) the friction of the material.¹⁰ The reported values of Poisson's ratio for rock ranges from 0.05 to 0.25 in various literature.⁸ Due to the fact that the minimum fracture extension pressure is not sensitive to Poisson's ratio, an average value of 0.15 is usually used.

Knowledge of rock mechanics is needed to explain what happens to a rock during hydraulic fracturing. All subsurface rocks are stressed in three directions due to the horizontal reactions to the weight of the overlying formations. Determining whether the horizontal or vertical stress is greater, depends on additional stresses imposed on the rock due to various geological movements that may have occurred in the area.⁵ These tectonic stresses determine whether the fracture plane will be

vertical, horizontal, or inclined as well as control the direction of the fracture. Due to these stresses on the rock and the strength of the rock itself, the rock is able to “stay together” during fracturing.

Pressure analysis of transient fluid flow must also be related to mechanical properties to correctly model the fracture propagation. Pressure analysis not only allows for the determination of fracture propagation, it also provides parameters which will be used in future design treatments. In investigating the material properties of the rock, it must be noted that the material balance is an important aspect of the pumping and closure phases of the fracturing treatment. It is known that hydraulic fracturing containment is related to linear elastic fracture mechanics. Three cases represent this effect: (1) the effect of different material properties for the pay zone and the barrier formation, (2) the characteristics of fracture propagation into regions of varying in-situ stress, and (3) the effect of hydrostatic pressure gradients on fracture propagation into overlying or underlying barrier formations.¹¹

There are many reasons why MHF techniques fail, including migration of the fracture into overlying rock or permeability caused by application of hydraulic fracturing fluid, loss of fracturing fluid into pre-existing cracks or fissures, or extreme errors in estimating the quantity of in-place gas.¹¹ Also poor estimates of in-situ permeability can result in failures that appear to be a result of the fracturing process. Hydraulic fracturing analysis is usually considered a three-dimensional problem. However, this results in a time consuming, costly, and complicated problem. Modeling the problem two-dimensionally makes it much simpler. The fracturing fluid is assumed to act over the entire length of the fracture.

For case (1), between the pay zone formations and the barrier formations, there are differences in mechanical properties. The question posed is what role do mechanical properties play in the containment of the hydraulic fracture to the pay zone. The stress intensity at the crack tip, nearest the interface varies as the fracture approaches the interface. Case (1) indicates the stiffness of the barrier formation as measured by the shear modulus is less than the stiffness of the pay zone.¹¹ For this case the stress-intensity factor approaches infinity as the ratio of the radius to the length approaches zero. Thus the closer the fracture gets to the interface, the easier it is to extend and the crack eventually will pass through the interface.

For case (2), analysis has been done, although simplified, that indicates an increase in fracture propagation pressure if the fracture extends into a barrier formation with higher in-situ stress. By accurately measuring the fracture propagation pressure, one can tell if the fracture has extended into the barrier zone. For this case, the stiffness of the barrier layer is greater than the stiffness of the pay zone. The stress-intensity factor approaches zero as the ratio of radius to length also approaches zero. This situation provides a barrier effect and tends to arrest the crack at the interface.¹¹

For case (3) a vertical plane-strain crack in an infinite medium is subjected to hydrostatic pressure loading. The externally applied loads are tectonic stresses. The magnitude of the tectonic stresses is a function of depth and thus uniaxial strain conditions prevail.¹¹ The important thing is that the desired upward or downward crack migration is possible. By adjustment of the hydraulic fracture fluid density, the

probability of producing horizontally propagating fractures can be maximized. To do this, the variation of in-situ stress with depth must be determined.

If the stiffness of the pay zones is less than the barrier layers, the hydraulic fracture will be contained, but if the opposite exists, barrier penetration will occur. The density of hydraulic fracturing fluid may control the migration of the hydraulic fracture, either upward or downward in an isotropic, homogeneous medium. If the fluid density gradient is greater than the minimum horizontal in-situ stress gradient, then downward migration is probable. If the fluid density gradient is less than the minimum horizontal in-situ stress gradient, then upward migration is probable. The mechanical properties of the pay zone and barrier formation, as well as the minimum horizontal in-situ stresses for these layers, play important roles in the prediction of hydraulic fracture containment.¹¹

2.5 Basic Relations

Various models are available from the literature to determine the fracture geometry. The most frequently reference models were the Perkins and Kern (PK), Khristianovic and Zheltov, and Geertsma and de Klerk (KGD). The elliptical cross-section as defined by Perkins and Kern was used in this research project. In the application of the fracturing pressure analysis, three basic relations must be considered. They are the material balance, fluid flow, and the compressibility of the fracture formation and the injected fluid. However, the fluid compressibility will be ignored for simplicity purposes of presenting the basic relations.

Although there are three aforementioned models, the pressure analysis and design requirements are always based on two expressions of material balance. At the end of pumping and the end of the closure time.⁸

The most important factor that must be considered is the in-situ stress field. Stress not only controls or influences most aspects of fracture behavior, but also influences the values of both reservoir properties and mechanical properties of rock.¹⁵ Generally increased confining stress results in an increase in strength and a decrease in permeability and porosity. The Khristianovitch-Zhel'tov / Geertsma-de Klerk model is generally considered applicable for fractures with a height / length ratio greater than one, and for this model, width is related to modulus by

$$w \sim (1/E)^{1/4} \quad (2-1)$$

This implies that fracture width is relatively insensitive to modulus.¹⁰

Propagation pressure is related by

$$(P - \sigma_c) \sim E^{1/4} \quad (2-2)$$

where σ_c is the confining stress.

Thus, it is inferred that rock with a high modulus causes higher pressure, which may alter the fracture geometry. For fractures with a height / length ratio less than one, the aforementioned relationships become

$$w \sim (\mu_i 4a_1^2 / E)^{1/4} \quad (2-3)$$

$$(P - \sigma_c) \sim Ew / 2a_1 \quad (2-4)$$

respectively.

2.6 In-situ Stress

By definition, in-situ stress is the stress state in a given rock mass at depth. The in-situ stress is greatly influenced by the overburden pressure. The stresses control the fracture azimuth and orientation (vertical or horizontal), vertical height growth, surface treating pressures, and other facets of fracture behavior.¹⁰ Closure stress σ_{\min} is defined as the minimum principal in-situ stress. This stress is located at the tip of the fracture, where the fracture width becomes zero. This stress counteracts with the closure pressure. Currently, the only reliable method of measuring in-situ stress is the hydraulic fracturing technique. This technique consists of two variations: the standard hydraulic fracture measurement and the step-rate / flowback procedure. When the hydraulic fracturing technique is conducted properly it can yield accurate estimates of the minimum principal in-situ stress and somewhat less accurate results of maximum horizontal in-situ stress. The procedure is to isolate the interval of interest with packers, to pump a small volume of low viscosity fluid into the formation to break it down, then shut in to measure the instantaneous shut-in pressure.¹⁰

Under these conditions it is accepted that

$$\sigma_{\min} = p_{is} \quad (2-5)$$

for a vertical fracture

$$\sigma_{\min} = p_{is} \quad (2-6)$$

where

p_{is} = instantaneous shut in pressure

For most oil and gas applications, however, it is impossible or impractical to conduct these tests in an openhole environment. Performing a stress measurement in a cased and perforated hole causes additional complications because of the effects of the casing, cement annulus, explosive perforation damage, and random perforation orientation.¹² Some tests show that under these conditions, accurate measurements of σ_{\min} can be made through the perforations.

The second stress measurement technique is the step-rate / flowback test procedure. It is a more applicable procedure for determining stress over a larger permeable interval. Fluid is injected into a previously initiated fracture at various flow rates, the “stabilized” pressure for each rate is recorded. For data interpretation see reference 10.

When performing rock fracturing, the rock properties of the most interest are the elastic properties. To simplify the theory and the calculations, the assumption is made that rock behaves as a linear elastic material. This assumption has allowed solutions to become essential in the development of hydraulic fracturing theory. It must be noted that many rocks behave in a nonlinear manner and the effects of this nonlinearity should be considered in certain instances. The basic assumption of the theory of linear elasticity is that the components of stress are linear functions of the components of strain.

Not only are rocks subjected to external forces, but they are also subjected to internal forces such as pore pressure and temperature. Due to in-situ conditions, volume changes cannot occur because impermeable rocks bound the reservoir. The impermeable rocks do not allow pore pressure to change.

2.7 Effect of In-Situ Stresses and Rock Properties on Geometry

The fracture azimuth, for an anisotropic field is perpendicular to the minimum, compressive principal in-situ stress. Thus the fracture follows the path of least resistance and therefore opens up against the smallest stress. In-situ stresses may single handedly control the fracture height. Experiments have been conducted to show the dominant effect of in-situ stresses opposed to rock properties. The importance of this test lies in the fact that in 20 separate tests, no major influence of material properties could be discerned.¹⁰ There are also documented laboratory tests that confer with this experiment. This was significant due to the past belief that the material properties played a vital role in fracture propagation. This finding tends to be favorable to the hydraulic fracturing industry due to the fact that many bounding layers are often soft materials like shale, which have high stresses.¹⁰

Many experiments have been done to determine the parameters that control hydraulic fracture containment. These experiments demonstrate that the stress contrast between the pay zone and bounding layer is the most important factor controlling fracture height. Material property interfaces are shown to have little effect.⁶ For the past 30 years hydraulic fracturing has been used to aid in the production of natural gas reservoirs. With the increasing depletion of conventional natural gas reserves, attention has been focused on producing gas from unconventional gas resources such as tight gas sands and Devonian shales.⁶ To stimulate these formations, massive hydraulic fracturing is used. To provide a high conductivity path for the gas to reach the wellbore, fractures longer than 4000 feet must be propagated in the low-permeability gas-bearing formation. It is very

important that these massive hydraulic fractures be contained within the pay zone. When referring to massive hydraulic fracturing in the tight gas sands, containment may refer to confinement of the fracture to specified intervals comprising both gas-bearing sandstone lenses and surrounding shale zones, or to the usual concept of confinement within a single reservoir zone.⁶

To control containment, the difference in elastic modulus between the reservoir rock and barrier rock usually is singled out as the primary mechanism. It has been observed that since the stress intensity factor at the tip approaches zero as a fracture in a lower-modulus material propagates toward a higher-modulus material, the fracture will tend to be arrested. Conversely, for fracture propagation in a higher-modulus material toward a lower-modulus material, it was observed that the stress intensity factor becomes large as the interface is approached and the fracture should break through the interface. The problem with this analysis is that everything is based on the strength intensity factor, which is defined as the strength of the square-root singularity in stress at the crack tip. Yet the nature of this singularity changes as an interface is approached.⁶ Once the crack reaches the interface, the strength intensity factor goes to zero and other singularities now control the fracture growth.

Experiments have been conducted, which show that differences in rock properties are insufficient in stopping fracture growth at an interface. Fracture propagation is effected by variations of in-situ stress. The layer of greater in-situ stress would provide an effective barrier because of the increase in the fracturing pressure necessary to continue propagating a fracture in this layer. The upward or downward migration of the fracture can be influenced by the hydraulic gradient of the fracturing

fluid relative to the vertical gradient of the minimum horizontal in-situ stress. Not only does the orientation of the minimum in-situ stress dictate the orientation of the fracture, but also steep gradients and discontinuities in the magnitude of the stress can act as barriers to fracture propagation.⁶

Fracture behavior around the interface has been important to determine whether material property differences between adjacent layers can act as a barrier to fracture propagation. In all the experiments, the fractures propagated upward through the interface into higher-modulus material. The results also showed that material property interfaces do not provide an effective mechanism for fracture containment. Since the fracturing pressure above the minimum in-situ stress level should be proportional to the elastic modulus, it will require, under similar conditions, considerably more pressure to fracture in a higher-modulus material than in a lower-modulus reservoir rock.⁶ Due to increasing viscous losses, the fracture may not propagate a great distance even if it has broken through the interface. The fracture will propagate along the path of least resistance, such as a lower modulus material, unless in-situ stresses or other parameters dictate otherwise.

Other experiments have been conducted to determine how the vertical and horizontal distribution of the in-situ stress effected the fracture growth and geometry. The minimum in-situ stress is equal to the closure pressure of the fracture after fracturing is completed. In-situ stress can vary widely over just a few feet as shown in Figure 2.1 below.

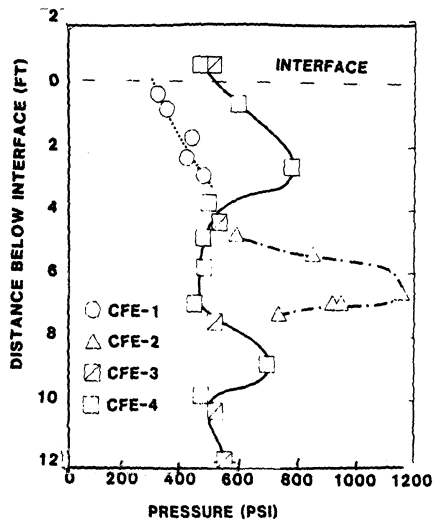


Figure 2.1
In-situ Stress Below Interface from Reference 6

Figure 2.1 shows that two significant in-situ stress irregularities exist below the interface, and in both cases, the in-situ stresses increase by a factor of two to three.⁶ With the variations in in-situ stress, the fracture usually propagated horizontally outward and upward into a material of much higher modulus and the growth stopped as it reached the region of greater in-situ stress. When the fractures were initiated above or below the in-situ stress peaks, the fractures propagated away from the high in-situ stress regions. The only exception to this is when the fractures were initiated close to the in-situ stress peaks. These often propagated through the high in-situ stress region, but this may be due to borehole effects.⁶ The tests that were initiated between the stress peak resulted in the fractures being contained in that area. The fractures were of rectangular shape since the regions of greater in-situ stress

contained them. Some of these fractures became so restricted that the pressure rose high enough for the fracture to break into higher regions.

The majority of evidence from the mineback of hydraulic fractures points to in-situ stress gradients as being the only mechanism capable of containing hydraulic fractures.⁶ Experiments have shown that discontinuities in the minimum principal in-situ stress, which may occur at faults and steep gradients in this stress can arrest fracture growth. To be able to control the fracture height, minifractures can be conducted to determine the stress distribution.

Mineback experiments have provided insight into the mechanisms responsible for controlling hydraulic fracture growth. Material property differences have been shown to be insufficient to arrest a fracture at an interface.⁶ Determination of the minimum in-situ stress is very important where containment is desired.

To be able to obtain deeply penetrating fractures, the in-situ stress contrasts must be applied to the stimulation designs. In general, the fracturing treatment design is based upon the assumption that the vertical height of the fracture is known and that this height remains constant from the wellbore to the point of deepest horizontal penetration. The contrast in in-situ stress between layers is the major influence of how adjacent rock layers will impede the vertical growth of a hydraulic fracture being propagated in the pay zone. As a fracture growing in the pay zone approaches the interface between the pay zone and the adjacent layer, its growth will be impeded if the minimum in-situ stress of the adjacent layer is greater than the minimum in-situ stress in the pay zone.¹³

Presently the only viable technique to determine in-situ stress at depths greater than 1000 ft is a small-scale hydraulic-fracturing operation. Tests have been performed to determine whether the stresses in particular the minimum horizontal stress applied to the specimens could be estimated by analysis of the pressure/time records obtained during the hydraulic fracturing of the specimens.¹³ Later, it was determined that this is not possible due to the fact that the fracture paths were somewhat tortuous and the pressures were measured in the wellbore, which would be a measure of some average stress acting perpendicular to the fracture.

The availability of in-situ stress data and the knowledge of the role that it and other rock mechanics parameters play in the physical process of fracture growth can lead to fracturing control.¹³ A successful stimulation design requires a knowledge of the in-situ stress field. It also requires knowledge of contrasts within relatively narrow ranges at well depth where the stimulation treatment is performed.

2.8 Fluid Loss from Hydraulically Induced Fractures

Accurate knowledge of fluid loss properties of the fracturing fluid is important for successful hydraulic fracturing treatments. Dynamic fluid loss refers to fluid leakoff from a fracture when a high flow velocity along the fracture exists at the point where fluid leakoff occurs. This is a normal situation since hydraulic fractures produce a long, narrow crack along which fluid flows at high velocities (up to several hundred feet per minute). High velocity is maintained far down the fracture even though volumetric flow rate decreases as the fracture becomes progressively more narrow.¹⁴ In a dynamic fluid loss test, fluid in a high stream of velocity moves past

the rock surface at the same time fluid enters the core. The high fluid velocity inhibits thick filter cake formation. Initially, pressure drop is totally dissipated across the core and fluid leakoff occurs as if no additive were present. Next, a filter cake begins to form and leakoff velocity is lower because some pressure drop occurs across the cake.¹⁴ Once the fluid leakoff velocity and the cake thickness become constant, steady state is reached. Flow velocity through the steady-state cake is dependent upon flow velocity across the rock surface, upon fluid and additive properties and upon rock pore size. Dynamic fluid loss tests provide the best method for simulation of the fluid loss process during hydraulic fracture operations.¹⁴ Through the use of the tests and a reasonable theoretical model for the rate of fracture growth, fracture length can be estimated.

Chapter 3

VELOCITY PROFILE MODELING

3.1 Steady Two Dimensional Laminar Flow Model for an Elliptic Fracture

During hydraulic fracturing of gas or oil bearing rock formation, a pad fluid gel is pumped under pressure in excess of the minimum in-situ stress, σ_{\min} . The rock shears in the direction perpendicular to σ_{\min} , which if below 2000 feet deep, is usually horizontal. This means that the fractures created will be in the vertical plane and radiate outward from the well casing. Initially these fractures are circular but if restrained in the vertical direction by stronger layers of containment rock, then the fracture becomes of constant height, h , and continues radially outward to a length, $L_f \gg h$.

3.2 Model Boundary Conditions

All fracture models are based on elastic rock deformation equations to relate hydraulic pressure to fracture width. The local pressure is calculated by inserting fluid frictional characteristics in the momentum equation and fluid loss and storage assumptions in the continuity equation. To solve these equations, boundary conditions must be defined. Most existing models use similar equations but different boundary conditions. For the user to evaluate the suitability of any model, its assumed boundary conditions must be clearly defined. The boundary conditions assumed in this analysis are as follows.

- 1) Uniform rock properties with known Young's modulus and Poisson's ratio thus E' ,

and a known minimum in-situ horizontal stress σ_{\min} , where $E' = \frac{E}{1-\nu^2}$

- 2) Fracture propagation within confined boundaries without slip, thus producing a fracture of constant height, h and varying elliptically in the vertical plane with width $w_{z,x}$, which reaches a maximum width $w_{m,x}$ in the middle and reduces to zero at the tips. The x -coordinate runs radially outward from the well casing and the z -coordinate is in the vertical direction. The subscripts of each variable indicate the direction of its variability.
- 3) As the fracture considered changes only gradually in width and is assumed to be of constant height, the components of velocity in the y and z -directions can be ignored. In this case the velocity vector has only a component in the x -direction which varies drastically with y and z position. From Euler's equation $\rho V dV = -dp$, it follows that the components of the pressure gradient in the y and z direction can be ignored, thus one can use the boundary condition that the pressure is uniform in the y - z plane, or dp/dx is the same at any x location. Then $|\vec{V}| = V_x$ but V_x varies along all three x , y , and z -axes. Along the y -axis, the flow has the same boundary conditions as Hagen-Poiseuille flow and therefore the velocity profile is parabolic with an averaged value, $V_{z,x}$, equal half the maximum centerline value. The next task is to compute $V_{z,x}$ along the x and z -axes. Within the majority of the fracture, it is assumed that the rock surface is covered with gel fluid. This is known as the cake effect and results in negligible fluid loss. This allows the use of constant flow rate, q_i (ft^3/s) = (q) , which equals the injected flowrate.

3.3 Pressure Gradient Derivation

For a fracture where the length, L_f far exceeds the height, the Sneddon¹⁵ model was selected as used by Perkins and Kern. Based on this model, the fracture is elliptical in the vertical z -direction and decreases in maximum width, $w_{m,x}$ as pressure drops. At the limit $x = L_f$, the fracture length, the fluid pressure is reduced to the minimum in-situ stress, which is $\sigma_{\min} = p_{L_f}$ and the maximum width of the fracture has reduced to zero. At any other station, $x < L_f$, the maximum width is given by

$$w_{m,x} = 2h \frac{p - S_{\min}}{E'} \quad (3-1)$$

E' is used rather than E due to the over burden pressure of the rock. The weight of the rock pushing down from above must be taken into account. E' and E are related by Poisson's ratio, ν . This results in an elliptical cross-section given by

$$\frac{z^2}{(\frac{1}{2}h)^2} + \frac{y^2}{(\frac{1}{2}w_{m,x})^2} = 1 \quad (3-2)$$

where y is

$$y = \frac{1}{2} w_{z,x} \Rightarrow y = \frac{1}{2} w_{m,x} \sqrt{1 - \left(\frac{z}{\frac{1}{2}h}\right)^2}$$

$$\text{Therefore } w_{z,x} = w_{m,x} \sqrt{1 - \left(\frac{z}{\frac{1}{2}h}\right)^2}$$

The area (A_x) is defined by

$$A_x = \int_{-0.5h}^{0.5h} w_{z,x} dz = \frac{p}{4} w_{m,x} h = w_{av} h \quad (3-3)$$

where $w_{av} = A_x/h$ is the average fracture width and $w_{m,x}$ is the centerline maximum width related to local hydraulic pressure p_x .

$$w_{m,x} = 2h \frac{p - S_{\min}}{E'} = \frac{4}{p} w_{av} \quad (3-4)$$

The following velocity profile analysis is based on the previous conclusion that the pressure gradient, dp/dx , is uniform in the y-z plane.

$$\frac{dp}{dx} = \frac{-f \frac{1}{2} r V_{z,x}^2}{D_H}$$

The hydraulic diameter, $D_H = 4 * \text{area} / \text{wetted wall perimeter}$

$$D_H = \frac{4w_{z,x} dz}{2dz} \Rightarrow D_H = 2w_{z,x} \quad (3-5)$$

Various shear stress models are used depending on the Reynolds number and fluid characteristics. For turbulent flow down the well tube, friction is a weak function of velocity, thus it can be assumed constant, and is given by Blasius for smooth pipes as

$$f = \frac{0.3164}{N \text{Re}^{0.25}}$$

The Reynolds number for Newtonian fluid is given by

$$N\text{Re} = \frac{rV_{z,x} D_H}{m} \quad (3-6)$$

For laminar flow inside a nearly parallel wall cross-section fracture, the velocity profile is parabolic. Using the Darcy friction coefficient, f , for a Newtonian fluid as given

$$f = \frac{64}{N \text{Re}} = \frac{64m}{rV_{z,x} D_H} \quad (3-7)$$

If the friction coefficient, f , were modified to account for the tortuous path caused by the rough fracture surface and averaged over the entire height, a simple correction factor ($r_f = f_{\text{experimental}}/f_{\text{lam}}$) could be applied as shown in Table 3.1 from reference 16.

Table 3.1 Comparison of Measured vs. Theoretical Friction Factors in Hydraulic Fracture

Test	Fluid	Flow Rate (gal/min)	Height (ft)	Apparent Viscosity (cp)	$r_t = f_{ex} / f_{lam}$
4	Water	10	10	1.0	1.39
5	Water	20	12	1.0	2.45
6	Water	30	12	1.0	2.75
7	Water	40	15	1.0	3.11
9	50 lbm gel	20	20	20	2.15
10	50 lbm gel	40	20	22	2.16
11	50 lbm gel	20	20	45	1.48

By limiting this analysis to “smooth” fractures, r_t can be assumed to equal 1. Applying the x component of the momentum equation gives

$$-\frac{dp}{dx} = \frac{1}{2} \mathbf{r} V_{z,x}^2 \frac{f_{lam}}{D_H} = \frac{1}{2} \mathbf{r} V_{z,x}^2 \left(\frac{64m}{\mathbf{r} V_{z,x} D_H^2} \right) = \frac{8mV_{z,x}}{w_{z,x}^2} = \frac{8mV_{m,x}}{w_{m,x}^2} \quad (3-6)$$

At any station x, these variables are constant, with the exception of $V_{z,x}$ and $w_{z,x}$, or

$$\frac{V_{z,x}}{V_{m,x}} = \left(\frac{w_{z,x}}{w_{m,x}} \right)^2 = 1 - \left(\frac{z}{\frac{1}{2}h} \right)^2 \quad (3-7)$$

As $w_{z,x}$ varies elliptically, then $V_{z,x}$ decreases parabolically from $V_{m,x}$ at the centerline down to zero at the tips where $z = \frac{1}{2}h$. The relationship between $(V_{m,x})$ and $(V_{av}) = q/A_x$ can be readily integrated to give

$$V_{av} = \frac{2 \int_0^{\frac{h}{2}} V_{z,x} w_{z,x} dz}{2 \int_0^{\frac{h}{2}} w_{z,x} dz} = \frac{V_{m,x} \int_0^{\frac{h}{2}} \left(1 - \left(\frac{z}{\frac{1}{2}h} \right)^2 \right)^{\frac{3}{2}} dz}{\int_0^{\frac{h}{2}} \left(1 - \left(\frac{z}{\frac{1}{2}h} \right)^2 \right)^{\frac{1}{2}} dz} = \frac{3}{4} V_{m,x} \quad (3-8)$$

As ($V_{m,x} = \frac{1}{2} V_{max}$), this means that perfectly smooth fracture walls result in a

$$\text{centerline velocity } V_{max} = \frac{\frac{4}{3} V_{av}}{\frac{1}{2}} = 2.66 V_{av} .$$

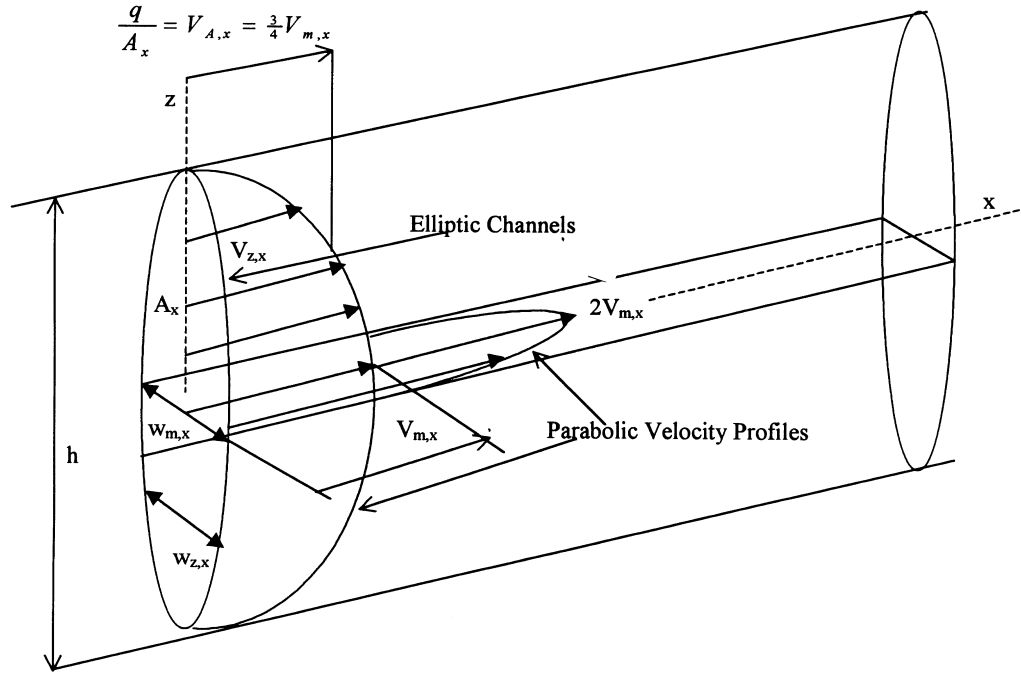


Figure 3.1
3D Velocity Profiles Caused by Friction

Apply the continuity equation in order to define flowrate (q).

$$q = \int_{-0.5h}^{0.5h} V_{z,x} w_{z,x} dz = \frac{-dp}{8m} \int_{-0.5h}^{0.5h} w_{z,x}^3 dz = \frac{-dp}{dx} \frac{3phw_{m,x}^3}{128m} \quad (3-9)$$

Solve for (dp/dx) as a function of the flow rate (q) and $w_{av} = \frac{p}{4} w_{m,x}$

$$-\frac{dp}{dx} = \frac{128mq}{3phw_{m,x}^3} = \frac{2p^2mq}{3A_x w_{av}^2} \quad (3-10)$$

Next determine the change in width ($w_{m,x}$) as a function of x . Take the derivative of Eq. (3-4) and equate it with Eq.(3-10).

$$\frac{dp}{dx} = \frac{E'}{2h} \frac{dw_{m,x}}{dx} = -\frac{128mq}{3phw_{m,x}^3} \quad (3-11)$$

Separate the variables and integrate from any station x to $x = L_f$, the end of the fracture where $p = \sigma_{\min}$ and $w_{m,x}=0$

$$\int_x^{L_f} -\frac{256mq}{3pE'} dx = \int_{w_{m,x}}^0 w_{m,x}^3 dw_{m,x} \quad (3-12)$$

gives

$$w_{m,x} = \left[\frac{1024mq(L_f - x)}{3pE'} \right]^{\frac{1}{4}} \text{ and } w_{m,o} = \left[\frac{1024mqL_f}{3pE'} \right]^{\frac{1}{4}} \quad (3-13)$$

The local centerline width defines the local average width

$$w_{av} = \frac{p}{4} w_{m,x} = \frac{p}{4} \left[\frac{1024mq(L_f - x)}{3pE'} \right]^{\frac{1}{4}} \quad (3-14)$$

as needed in the transient flow computer program to calculate the steady state areas as anyone station

$$A_x = hw_{av} = \frac{ph}{4} \left[\frac{1024mq(L_f - x)}{3pE'} \right]^{\frac{1}{4}} \quad (3-15)$$

which causes an increase in velocity throughout the fracture as found from $V_x = \frac{q}{A_x}$,

assuming no leakage until near the end of the fracture. The steady state pressure is then most conveniently calculated by using the known width using Eq. 3-1, which gives

$$p - s_{\min} = \frac{2w_{av}E'}{ph} \quad (3-16)$$

With the fracture centerline width variation known as a function of x, one can determine the fracture volume, Vol_f and solve for its length, L_f .

$$Vol_f = \int_0^{L_f} A_x dx = \frac{ph}{4} \int_0^{L_f} w_{m,x} dx = \left(\frac{3p^2 E' h}{5120mq} \right) \left(\frac{1024mqL_f}{3pE'} \right)^{\frac{5}{4}} \quad (3-17)$$

Both Δp and Vol_f can be measured during fracturing at constant q. As Δp increases in bottom hole pressure and assuming two equal and opposite fractures, the fracture volume Vol_f can be computed. $Vol_f = Vol \text{ pumped} * \text{Fluid Efficiency}$. The length (L_f) can be calculated for a given flow rate q.

$$L_f = \frac{\left(\frac{5Vol_f}{ph} \right)^{\frac{4}{5}}}{\left(\frac{1024mq}{3pE'} \right)^{\frac{1}{5}}} \quad (3-18)$$

As (q) may not be constant throughout the fracturing process, it is better to write an equation for (Δp) as a function of the measurable volume. By combining Eqs. 3-4 and 3-16, Δp can be written as

$$\Delta p = p - s_{\min} = \left(\frac{E'}{2h} \right) \left(\frac{1024mqL_f}{3pE'} \right)^{\frac{1}{4}} \quad (3-19)$$

If (q) is constant, then the fracture volume (Vol_f) grows linearly with time and combining Eqs 3-17 and 3-19 Δp can be written as

$$\Delta p = \left(\frac{E'}{2h} \right) \left(\frac{5120mqVol_f}{3p^2 h E'} \right)^{\frac{1}{5}} \propto t^{\frac{1}{5}} \quad (3-20)$$

Thus plotting ($\log \Delta p$) versus ($\log t$) gives a slope of 1/5 as shown in Fig 3.2.

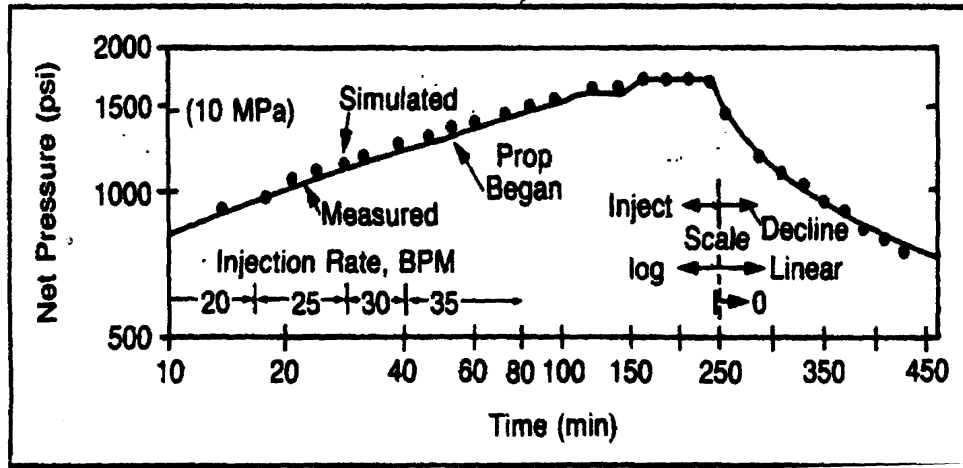


Figure 3.2
Measured and Simulated Net Pressure: Opening Natural Fissures from Reference 17

3.4 Errors Associated With Assuming V_{av} Across Fracture

The following analysis calculates the errors associated with the use of V_{av} and w_{av} instead of using $V_{m,x}$ and $w_{m,x}$. Equate the pressure gradient from both Eq. (3-4) and the momentum Eq. (3-8).

$$-\left(\frac{dp}{dx}\right)_{av} = \frac{8mV_{av}}{w_{av}^2} = \frac{8mq}{hw_{av}^3} = -\left(\frac{pE'}{8h}\right)\frac{dw_{av}}{dx} = 1.22\left(-\frac{dp}{dx}\right) \quad (3-21)$$

This shows that the pressure gradient based on the average velocity is 22% higher than the pressure gradient based on the actual 3D-velocity profile. Separating variables and integrating this average velocity model from x to L_{fav}

$$L_{fav} - x = \left(\frac{E'}{pmq}\right)w_{av}^4 \text{ then } w_{av} = \left(\frac{pmq(L_{fav} - x)}{E'}\right)^{\frac{1}{4}} \quad (3-22)$$

Compare the volume (Vol_{av}) based on average velocity (V_{av}) to that based on the parabolic velocity profile ($V_{m,x}$).

$$Vol_{av} = \int_0^{L_{fa}} hw_{av} dx = \left(\frac{4E'h}{5pm_l} \left(\frac{pm_l L_{fav}}{E'} \right)^4 \right)^{\frac{5}{4}} \quad (3-23)$$

Equating this volume to that from Eq. (3-18) provides the ratio of fracture length estimates based on the average and actual velocity profiles.

$$\frac{L_{fav}}{L_f} = \left(\frac{p}{4} \right)^{\frac{4}{5}} \left(\frac{1024}{3p^2} \right)^{\frac{1}{5}} = 1.67 \quad (3-24)$$

These results are obtained by assuming quasi-steady state and the steady flow continuity equation. With the derived values for width, $w_{m,x}$ and pressure, $(p - \sigma_{min})$ both as a function of distance from the fracture tip, $(L_f - x)$ the non-steady state of fracture length growth as a function of time may be addressed.

Assuming no change in boundary conditions in time Δt , the entire fracture with identical geometry and pressure is shifted radially outward by a distance $\Delta x = dL_f$. Thus, the only change in fracture geometry with time occurs at the well inlet side. This analysis was done to show the difference when using average velocity opposed to actual velocity. The following computer program in Chapter 4 illustrates how using average velocity inside the fracture with a constant fracture friction coefficient causes the pressure signal to dampen out.

CHAPTER 4

ACOUSTIC WELL CHARACTERISTIC ANALYSIS

4.1 Acoustic Analysis

The following is a computer program to calculate the acoustic wave pressure oscillation in a typical well pipe and fractures. The flow boundary conditions are flow reduction from 14 to 7 bpm, within half the tube period or within 4 seconds. The configuration selected was based on rounded off data from Halliburton Job ticket 100723, February 4, 1998. The fracture model was assumed to be of uniform width, ($w = \text{Vol}/(h \cdot L_f)$), with a rectangular cross section. This simple well model is to demonstrate the use of the method of characteristics. The program becomes complex unless the geometry selected is simple. The fracture length was assumed to be equal to one tenth that of the well tubing. Power Law equations were used for tube friction loss calculations. For turbulent flow in the tube, the Lord/McGowan model from reference 18, provides the turbulent friction coefficient ($f_{D_{\text{Gel}}} = \sigma^*(f_{D_{\text{water}}})$), where

$$S = e^{\left[-2.38 + \frac{8.024 + 0.2365(G)}{V} + 0.1639 \ln(G) + 0.028(\text{Prop})(e^{\frac{1}{G}}) \right]} \quad (4-1)$$

This sigma equation is calibrated on a reference coefficient, ($f_{D_{\text{water}}}$) defined differently from before by

$$(f_{D_{\text{water}}}) = \left(\frac{4 \cdot 0.046}{N \text{Re}^{0.2}} \right), \text{ where } N \text{Re} = \frac{rVD_H}{m_{\text{water}}}$$

Then the turbulent friction coefficient ($f_{D_{\text{Gel}}} = \sigma^* f_{D_{\text{water}}}$).

Inside the fracture laminar flow was assumed, thus using n' and K' to find $N \text{Re}'$.

$$NRe' = \frac{rV^{2-n'} D_H^{n'}}{K'8^{n'-1} \left(0.75 + \frac{0.25}{n'}\right)^{n'}} \quad (4-2)$$

This gives the Darcy friction coefficient as $\frac{64}{NRe'}$.

The method of characteristics requires tube (1) and fracture (2) to be divided into an even number of segments. Selecting $\Delta x = 400$ ft, then the tube has

$$N1 = \frac{8000}{400} = 20 \text{ segments and the fracture } N2 = \frac{800}{400} = 2 \text{ segments. The time}$$

increment $(\Delta t) = \Delta x/c = 400/4000 = 0.1$ seconds. The end stations are: 1,NS = N1 + 1 = 21 and 2,NS = N2 + 1 = 3. The example program is written in Quick Basic and is found in Appendix C.

4.2 Procedure

$N = 1$ is the beginning of the first segment and NS is the end of the last segment. Thus P1,1 and P1,NS are the pressures at the inlet and exit of the tube respectively and P2,1 and P2,NS are the pressures at the inlet and exit of the fracture respectively. The characteristic impedance is defined as $(B) = c/(gA)$ and the

resistance coefficient is defined as $(R) = fD \frac{\left(\frac{\Delta x}{D}\right)}{(2gA^2)}$. At each node, (i), H, Q, CP,

CM, BP, and BM need to be determined by the method described in Chapter 1.

4.3 Steady Flow Boundary Conditions

From job ticket 100723 obtain the steady flow fracture end static pressure $P_{NS2} = 6400$ psi which is used for the minimum in-situ stress in this example program. Assume all flow leaks out near the fracture end with dynamic pressure $\frac{1}{2} \rho (V_{NS2})^2$, which is assumed constant throughout this rectangular fracture. Here the fracture width is not calculated from Eq. (3-14) but is taken from job ticket 100723, which number is based on a much higher flow rate during fracturing. It was assumed that it takes more time for the rock to relax back to a new equilibrium fracture width, than there was time to do so. The fracture inlet static pressure $P_{2,1} = 6400 - dff$, where dff (psi) is the fracture friction pressure loss. The well bottom pressure = $P_{1,NS1}$. These pressures are related by $P_{2,1} = P_{1,NS1} - \frac{1}{2} \rho (V_{perf})^2$. The perforation dynamic pressure was assumed lost. Gravity was also ignored in all calculations. The tube inlet static pressure equals $P_{1,1} = dft + \frac{1}{2} \rho (V_{perf})^2 + dff + (6400 \text{ psi} = \text{in-situ stress})$.

4.4 Transient Flow Boundary Conditions

Thirty-two data points per harmonic cycle are sufficient to graph the transient wave shape. Using the minimum number of required data points to minimize the length of the program. The flow rate was readily controlled by RPM of the positive displacement pumps. If the flow rate is reduced in time = $\frac{1}{2} q * \tau_t$ (where τ_t is the tube period for the natural frequency), then the reflected wave is a damped harmonic. Therefore when $Q_{1,1}$ is reduced by ΔQ during $0 < t < (\frac{1}{2} \tau_t = 4\text{sec})$ it is given by $Q_{1,1} = \Delta Q - \frac{1}{2} \Delta Q * (1 - \cos(\pi t / (\frac{1}{2} \tau_t)))$. $H_{1,1}$ will drop accordingly. $Q_{2,1} = (V_{perf})$

* CdAp, where $V_{perf} = \sqrt{\frac{(P1, NS1 - p2,11) * 2}{r}}$. The P2,1 pressure signal input to the

fracture is reflected at the fracturing surface tip, like an open reservoir with constant head equal σ_{min} . Such a boundary condition gives the most damped fracture pressure pulse. The reflected signal arrives at 0.4 seconds, ($\frac{1}{2} \tau_f$), later. Only if one is able to determine the natural frequency inside the fracture, τ_f , can one estimate the fracture length from $L_f = 0.25 * \tau_f * c$.

4.5 Well Tube Casing and Fracture Data

Table 4.1 Tube Data

Tube Length, L_t (ft) =	8000	G = gel (lb/Mgal)	20
Tube Inside Diameter (inch) =	2.441	Prop (lb/gal)	0
A (ft ²) =	0.032498	Lord /McGowan NRe water =	886103.6123
Steady State Q (bpm)	14	Lord McGowan sigma	0.207492288
Q(ft ³ / sec) (1bpm * 0.09359 ft ³ /sec/bpm) =	1.31026	water fB =	0.011893808
Velocity (ft/sec)=	40.31759	fD(Gel) =	0.002467873
Fluid density (slugs/ft ³) =	1.946	Characteristic friction coefficient R1=	71.34845538
Gel with n' =	0.789	Characteristic impedance coefficient B1=	3822.444352
$K'(lb^*sec^n / ft^2) =$	6.14E-04	Friction loss in tube dftpsf (psf)	153507.0214
Wave speed, c (ft/sec) =	4000	Loss dftxpsf in ΔX (psf)	7675.351068
delt=time step (sec)	0.1	Loss head ΔH in ΔX (ft)	122.4896917
Select ΔX (ft)=	400	Tube dynamic pressure (psf)	1581.619133
Number of Tube stations $N1=L_t / \Delta X=$	20	Delperf, dynamic pressure perforation (psf) =	8649.394208
Calculate effective perforation area		Pi	3.141592
50 perforations .28", Cd.65		Gravity, g (ft/s ²)	32.2
Gives Net Area CdAp =	0.013897		
Tube period $\tau_t = 4L_t/c$ (sec)	8		

Table 4.2 Fracture Data

Fracture length, L_f (ft) =	800	$NRe' =$	228.2749156
Vol of both fract.=Vol pumped*F.E.	788	FD (fracture) = $64/NRe'$	0.2803637
Each fracture has Vol (ft ³)	394	Alternate assumed fD (fracture) =	0.2803637
Fracture height h (ft) =	70	Characteristic friction coefficient $R2 =$	510.2056303
Fracture width $w = Vol/(h*L_f)$ (ft)=	0.007036	Characteristic impedance $B2=$	252.2306649
$D_H =$ hydraulic diameter (ft) = $2w=$	0.014071	P_{insitu} (psi)	6400
$A = w*h$ (ft ²) =	0.4925	P_{insitu} (psf)	921600
Steady state $Q = Q_{tube} / 2$ (bpm)	7	H_{insitu} (ft)	14707.66599
Steady state Q (ft ³ /sec)	0.65513	Friction pressure loss $dfpsf =$	27442.83186
Velocity (ft/sec)=	1.330213	Loss $dfxpsf$ per ΔX (psf)	13721.41593
Fluid density (slugs/ft ³)	1.946	Tube inlet pressure $P1,1$ (psf)	1111199.247
Gel with $n' =$	0.789	Tube inlet head $H1,1$ (ft)	17733.44984
$K' (lb_f*sec^n/ft^2) =$	6.14E-04		
Wave speed, c , (ft/sec) =	4000		
Number of stations $N2 = L_f / \Delta X =$	2		

The reason for this analysis is to determine if there is a need to use actual velocity rather than average velocity in the computer program. Using the aforementioned input data from Table 4.1 and Table 4.2 from the Halliburton job ticket, the pressure wave signals were graphed and are found in the following chapter.

CHAPTER 5

RESULTS AND DISCUSSION

5.1 Steady State Results

These results were obtained by assuming quasi-steady state and the steady flow continuity equation. The values for the width, $w_{m,x}$, and pressure, $(p_x - \sigma_{min})$, both as a function of distance from the fracture tip, $(L_f - x)$, have been derived. The following tables display the results from the Qbasic program in Chapter 4. The program was run for 30 seconds and the flow rate dropped from 14 to 7 bpm in 4 seconds where it was held constant at 7 bpm after the first 4 seconds. This chapter also includes the figures of the transient pressure waves in the tubing and fracture caused by the flow rate change.

Table 5.1 Steady State Tube Data

Station I	H(ft)	Q(ft ³ /s)	P (psi)
1	17733.45	1.31026	7716.66144
2	17610.96	1.31026	7663.360391
3	17488.47	1.31026	7610.059342
4	17365.98	1.31026	7556.758293
5	17243.49	1.31026	7503.457244
6	17121	1.31026	7450.156195
7	16998.51	1.31026	7396.855146
8	16876.02	1.31026	7343.554097
9	16753.53	1.31026	7290.253048
10	16631.04	1.31026	7236.951999
11	16508.55	1.31026	7183.65095
12	16386.06	1.31026	7130.349901
13	16263.57	1.31026	7077.048851
14	16141.08	1.31026	7023.747802
15	16018.59	1.31026	6970.446753
16	15896.1	1.31026	6917.145704
17	15773.61	1.31026	6863.844655
18	15651.13	1.31026	6810.543606
19	15528.64	1.31026	6757.242557
20	15406.15	1.31026	6703.941508
1NS	15283.66	1.31026	6650.640459

Table 5.2 Steady State Fracture Data

Station	H(ft)	Q(ft ³ /s)	P (psi)
1	15145.62	0.65513	6590.575221
2	14926.64	0.65513	6495.287611
2NS	14707.67	0.65513	6400

5.2 Transient Flow Results

Table 5.3 Transient Flow Calculations for the Well Tube

B1 =	3822.444	R1 =	71.34845538		
Cv =	0.006219				
Time T	CM1,1	BM1,1	H1,1	Q1,1	CP1,2
0			17733.44984	1.31026	
0.1					22741.84578
0.2	12602.56	3915.929379	17717.65742	1.3062271	
0.3					22710.63794
0.4	12602.2	3915.648499	17669.93744	1.2942278	
0.5					22617.05129
0.6	12600.39	3914.812495	17590.04042	1.2745576	
0.7					22461.96574
0.8	12595.79	3913.441301	17478.59043	1.2477007	
0.9					22247.85674
1	12587.19	3911.567872	17337.08384	1.2143184	
1.1					21978.74847
1.2	12573.59	3909.237434	17167.85912	1.1752329	
1.3					21660.12139
1.4	12554.19	3906.506443	16974.03798	1.1314064	
1.5					21298.77598
1.6	12528.43	3903.44126	16759.43928	1.0839182	
1.7					20902.6561
1.8	12495.99	3900.116592	16528.4688	1.0339375	
1.9					20480.63719
2	12456.81	3896.613709	16285.9891	0.982695	
2.1					20042.28605
2.2	12411.01	3893.018479	16037.17462	0.9314525	
2.3					19597.60014
2.4	12358.94	3889.419285	15787.35791	0.8814718	
2.5					19156.735
2.6	12301.09	3885.904841	15541.87321	0.8339836	
2.7					18729.72912
2.8	12238.07	3882.561993	15305.90358	0.7901571	
2.9					18326.23521
3	12170.57	3879.473533	15084.33726	0.7510716	
3.1					17955.26653
3.2	12099.36	3876.716108	14881.6385	0.7176893	

Table 5.4 Transient Flow Calculations for End Tube Station and Fracture

		Fracture Transient Solution				
		R2 =	510.2056	B2 =	252.2307	
H1,NS1	Q1,NS1	Time T	H2,1	Q2,1	H2,NS2	Q2,NS2
15283.66	1.31026	0	15145.62	0.65513	14707.67	0.65513
		0.1				
15283.66	1.31026	0.2	15145.62	0.65513	14707.67	0.65513
		0.3				
15283.66	1.31026	0.4	15145.62	0.65513	14707.67	0.65513
		0.5				
15283.66	1.31026	0.6	15145.62	0.65513	14707.67	0.65513
		0.7				
15283.66	1.31026	0.8	15145.62	0.65513	14707.67	0.65513
		0.9				
15283.66	1.31026	1	15145.62	0.65513	14707.67	0.65513
		1.1				
15283.66	1.31026	1.2	15145.62	0.65513	14707.67	0.65513
		1.3				
15283.66	1.31026	1.4	15145.62	0.65513	14707.67	0.65513
		1.5				
15283.66	1.31026	1.6	15145.62	0.65513	14707.67	0.65513
		1.7				
15283.66	1.31026	1.8	15145.62	0.65513	14707.67	0.65513
		1.9				
15283.66	1.31026	2	15145.62	0.65513	14707.67	0.65513
		2.1				
15281.43	1.305849	2.2	15144.33	0.652925	14707.67	0.65513
		2.3				
15274.23	1.292759	2.4	15139.86	0.64638	14707.67	0.654313
		2.5				
15261.26	1.271282	2.6	15131.32	0.635641	14707.67	0.651339
		2.7				
15242.27	1.241755	2.8	15118.29	0.620877	14707.67	0.645364
		2.9				
15217.39	1.204602	3	15100.72	0.602301	14707.67	0.635863
		3.1				
15187.05	1.160362	3.2	15078.79	0.580181	14707.67	0.622517

5.3 Figure and Table Results and Explanation

For steady state analysis the following equation was used

$$H_{1,1} = \frac{s_{\min}}{rg} + f_f \left(\frac{Q}{2} \right)^2 + \frac{V_{\text{perf}}^2}{2g} + f_t \frac{Q^2}{2gA_t^2}$$

This summation is the minimum in-situ stress plus the friction loss through the fracture plus the dynamic head loss through the perforations plus the friction loss through the tube. Gravity terms could be ignored as all calculations were done in feet of head, which is not effected by pipe or fracture altitude or orientation.

For transient analysis, Figure 5.1 represents the equivalent pressure head readings at the tube inlet. The period of this graph, 8 seconds, represents the time it takes for the pressure wave to travel twice from tube inlet to end of tube and back. After four oscillations the tube pressure wave dampens out due to friction. Figure 5.2 represents the pressure head readings at the fracture inlet. The initial straight line denotes the time it takes for the pressure wave to reach the fracture inlet. The pressure waves shown are calculated just outside the casing wall. Note that the fracture friction is so high, that the ten times higher frequency pressure waves, created fracture internal wave reflections that were not visible. This may be due to the use of a constant value for the friction coefficient, and V_{av} as a too low velocity. To demonstrate the occurrence of the ten per cycle fracture internal wave reflections the friction coefficient was artificially lowered by a factor of 100. Now the pressure waves created inside the fracture become visible. This is shown in Figure 5.3. Due to the fracture length being 10 times shorter than the tube length, 10 oscillations occur inside the fracture for every one oscillation inside the tubing. Figure 5.4 represents the tube inlet flow rate boundary condition. The flow rate drops from 14 to 7 bpm in 4 seconds.

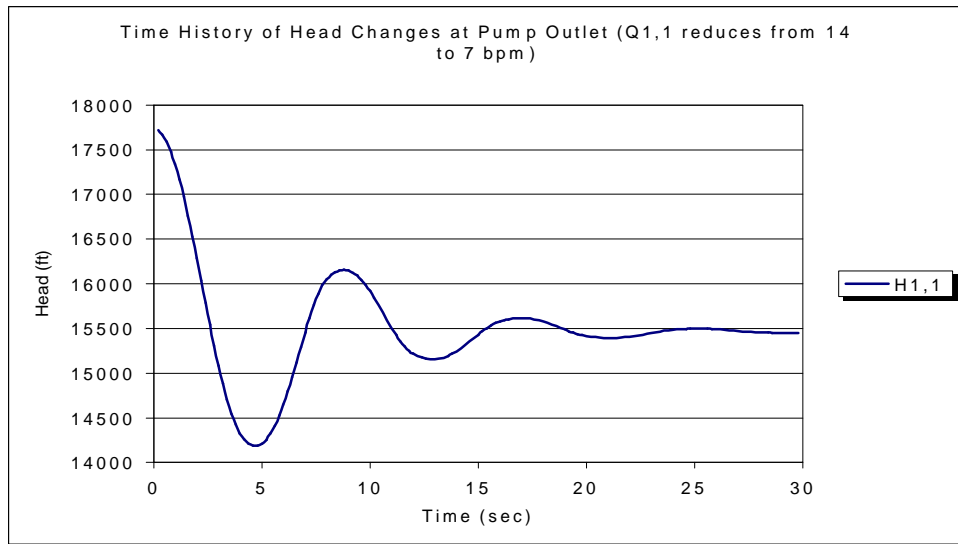


Figure 5.1
H1,1 vs. Time

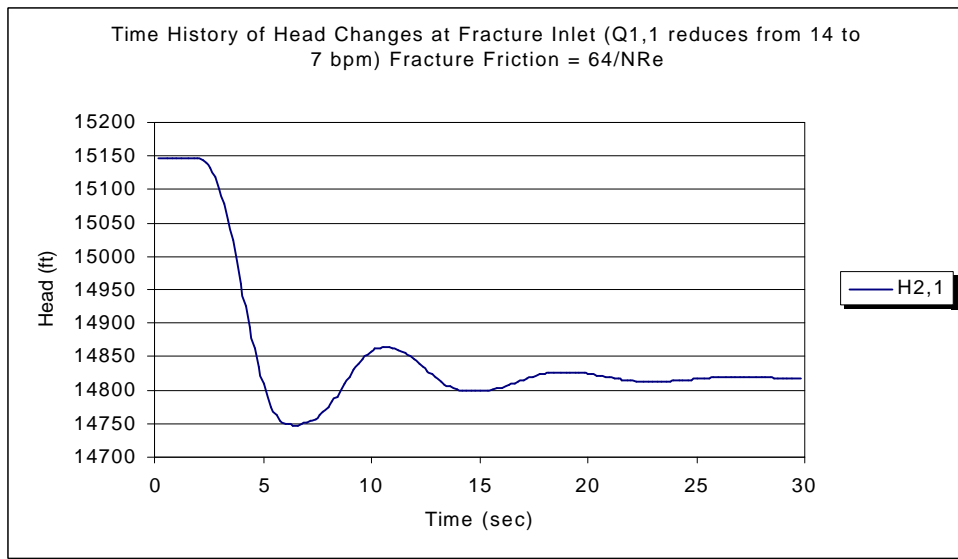


Figure 5.2
H2,1 vs. Time With Fracture Friction = $\frac{64}{N Re}$

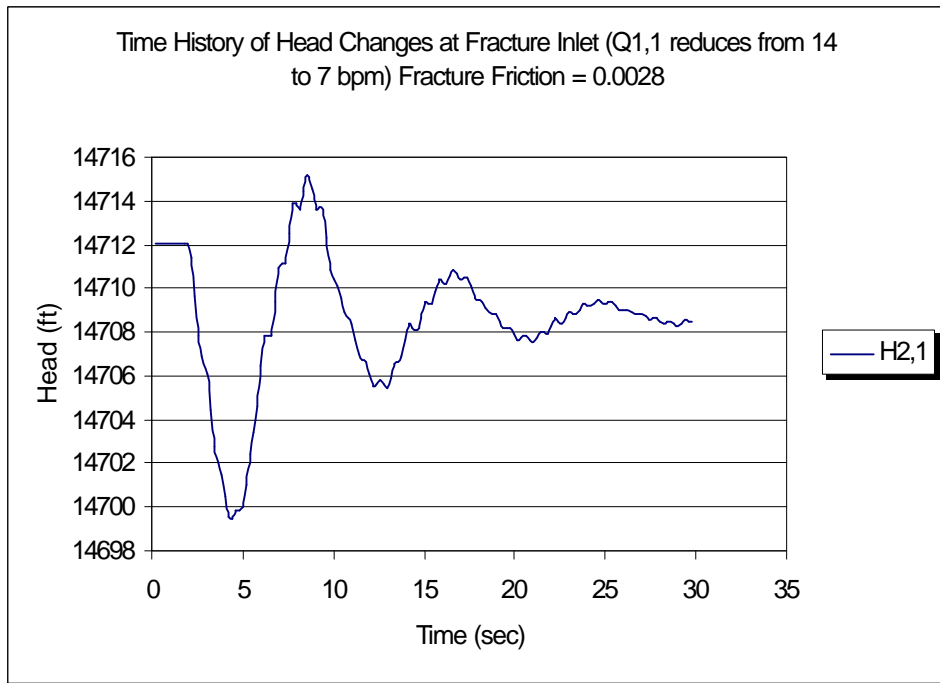


Figure 5.3
H2,1 vs. Time With Fracture Friction = 0.0028

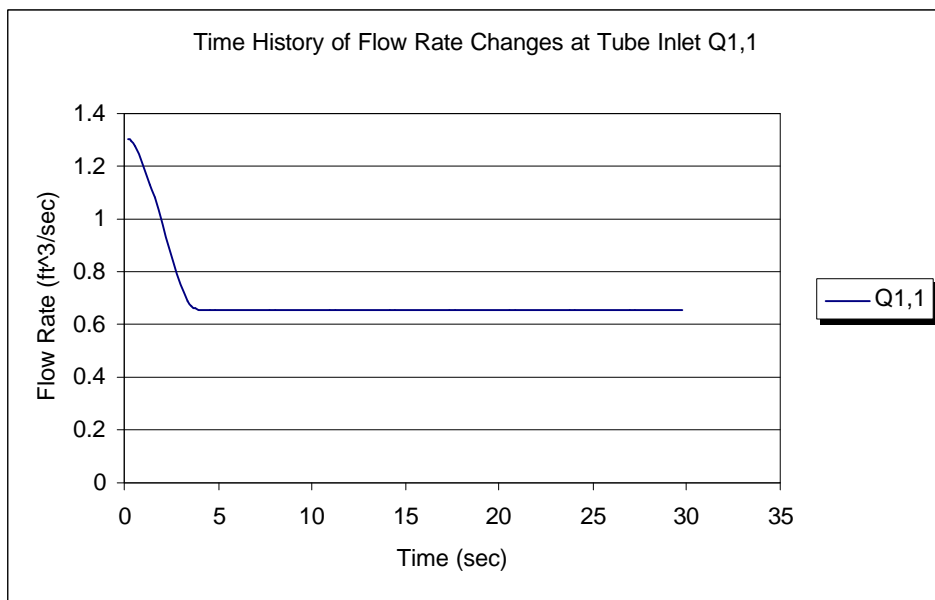


Figure 5.4
Fluid Flow Rate vs. Time

CHAPTER 6

CONCLUSIONS AND RECOMMENDATIONS

6.1 Conclusion

Equation (3-24) indicates that the change in hydraulic diameter over the height of the fracture has a profound effect on the difference in velocity between the maximum centerline value and the average value. In this case basing the length on the 2D velocity inside the fracture overestimates its length by 67%. As was seen from Table 1.1, the various models currently in use are based on the 2D-velocity model and have similar order of magnitude differences. If the effect of increasing relative roughness, RMS is added in the form of r_t as a function of distance from the centerline, z , then the 3D effect is likely to double. The tortuous path factor needs to be modeled. The significant variation in the 3D velocity applies to Newtonian and gel fluids without proppant. It is likely to have a profound effect on the transport and penetration of proppant. This analysis demonstrates the need to continue investigation the aspects of friction in the acoustic analysis of velocity transients inside a fracture. The presence of these waves was demonstrated by artificially lowering the friction coefficient by 100, which rendered the fracture internal reflections visible.

6.2 Recommendations for Future Study

- 1) The computer program needs to be modified to account for the fracture velocity profile and the equilibrium fracture width. This might result in a reduced friction coefficient, causing the fracture acoustic oscillation not to be critically damped.
- 2) Further study needs to be done on the tortuous path and how it effects the acoustic characteristics of the fracture and proppant transport.
- 3) Various signal-processing techniques, which will be needed to isolate the fracture characterizing oscillations from those inside the well tubing needs to be investigated.

REFERENCES

- 1) Geertsma, J. "Two-Dimensional Fracture-Propagation Models," pp. 81, Recent Advances in Hydraulic Fracturing, SPE 1989.
- 2) Nolte K. G. and Smith M. B. "Interpretation of Fracturing Pressures," pp. 131 Volume 1, SPE Reprint Series No. 28 Hydraulic Fracturing-2, 1990
- 3) Chaudhry, M. H., "Applied Hydraulic Transients" Van Nostrand Reinhold Co., 1979.
- 4) Wylie, B. E. and Streeter, V. L., "Fluid Transients in Systems" Prentice Hall, 1993.
- 5) Martinez, S. J., Steanson, R. E. and Coulter, A. W. "Formation Fracturing," pp. 46, Volume 1, SPE Reprint Series No. 28 Hydraulic Fracturing-1, 1990.
- 6) Warpinski, N. R., Schmidt, R. A. and Northrop, D., "In-Situ Stresses: The Predominant Influence on Hydraulic Fracture Containment," pp. 100 Volume 1, SPE Reprint Series No. 28 Hydraulic Fracturing-1, 1990.
- 7) Geertsma, J. and de Klerk, K., "A Rapid Method of Predicting Width and Extent of Hydraulically Induced Fractures," pp. 73, Volume 1, SPE Reprint Series No. 28 Hydraulic Fracturing-1, 1990.
- 8) Perkins T. K. and Kern L. R. "Width of Hydraulic Fractures," pp. 60, Volume 1, SPE Reprint Series No. 28 Hydraulic Fracturing-1, 1990.
- 9) Dobkins, T. A., "Improved Methods To Determine Hydraulic Fracture Height," pp. 123, Volume 2, SPE Reprint Series No. 28 Hydraulic Fracturing-1, 1990.
- 10) Warpinski, N. R. and Smith, M. B., "Rock Mechanics and Fracture Geometry," pp. 57, Recent Advances in Hydraulic Fracturing, SPE 1989.
- 11) Simonson, E. R. and Abou-Sayed, A. S., Clifton, R. J., "Containment of Massive Hydraulic Fractures" pp. 84 Volume 1, SPE Reprint Series No. 28 Hydraulic Fracturing-1, 1990.
- 12) Daneshy, A. A., Slusher, G. L., Chisholm, P. T. and Magee, D. A., "In-Situ Stress Measurements During Drilling," pp. 153, Volume 1, SPE Reprint Series No. 28 Hydraulic Fracturing-1, 1990.
- 13) Voegele, M. D., Abou-Sayed, A. S. and Jones, A. H., "Optimization of Stimulation Design Through the Use of In-Situ Stress Determination," pp. 112 Volume 1, SPE Reprint Series No. 28 Hydraulic Fracturing-1, 1990.

- 14) Williams, B. B., "Fluid Loss from Hydraulically Induced Fractures," pp. 282 Volume 1, SPE Reprint Series No. 28 Hydraulic Fracturing-1, 1990.
- 15) Sneddon I. N. "The Opening of a Griffith Crack under Internal Pressure," pp. 262, Proc. Roy. Soc. (1946) A, 187.
- 16) Veatch Jr. R. W., Moschovidis Z. A. and Fast R. C. "An Overview of Hydraulic Fracturing," pp. 1, Recent Advances in Hydraulic Fracturing, SPE 1989.
- 17) Economides M. J. and Nolte K. C. "Reservoir Stimulation," Prentice Hall, 1989
- 18) Lord, D. L. and McGowan, J. M., "Real Time Treating Pressure Analysis Aided By New Correlation," SPE-15367, Presented in New Orleans, LA October 5-8, 1986.

APPENDIX A

Derivation of Pressure Gradient for Non-Newtonian Fluid

Initial Condition

For steady state analysis the momentum equation gives

$$\frac{dp}{dx} = \frac{-f \frac{1}{2} \rho V^2}{D_H}$$

The hydraulic diameter, $D_H = 4 * \text{area} / \text{wetted wall perimeter}$

$$D_H = \frac{4w_{z,x} dz}{2dz} \Rightarrow D_H = 2w_{z,x} \quad (1)$$

Inside the fracture the flow is laminar with Darcy friction coefficient.

$$f_{x,z} = \frac{64}{NRe'} \quad \text{for a power law fluid or } f_{x,z} = \frac{64}{NRe} \quad \text{for a Newtonian fluid} \quad (2)$$

where NRe' is the power law Reynolds number. The equation for the power law Reynolds number is

$$NRe' = \frac{\rho V^{2-n'} D_H^{n'}}{K' 8^{n'-1} \left(0.75 + \frac{0.25}{n'} \right)^{n'}} \quad (3)$$

where ρ is the fluid density, V is the velocity, D_H is the hydraulic diameter, and n' and K' are the power law coefficients. The geometry analyzed is for 2 equal and opposite rectangular fractures near completion of the fracture where the change in fracture length, L , can be ignored during transient flow process. This is done to avoid accounting for moving boundaries and f is proportional to $1/V$ thus, it should not be assumed constant. Based on the Perkins model, the fracture is elliptical in the vertical z -direction and decreases in maximum width, $w_{m,x}$ as pressure drops. At the limit $x = L_f$, the fracture length, the fluid

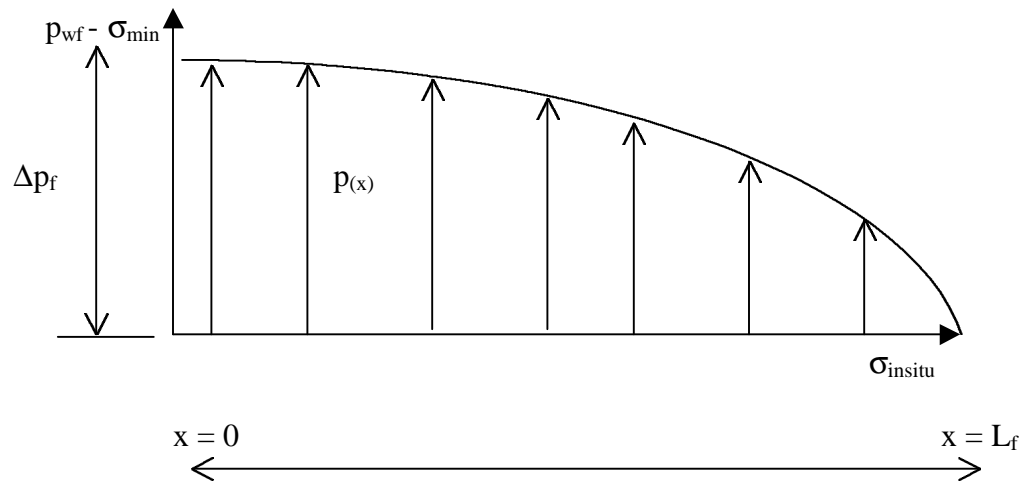
pressure has reduced to the minimum in-situ stress, which is $\sigma_{\min} = p_{L_f}$ and the maximum width of the fracture has reduced to zero. At any other station $x < L_f$ it is given by

$$w_{m,x} = 2h \frac{p - s_{\min}}{E'} \quad (4)$$

where

$$E' = \frac{E}{1 - \nu^2}$$

Pressure Distribution



The equation for an ellipse is

$$\frac{z^2}{\left(\frac{1}{2}h\right)^2} + \frac{y^2}{\left(\frac{1}{2}w_{m,x}\right)^2} = 1 \quad (5)$$

where y is given by

$$y = \frac{1}{2} w_{z,x} \Rightarrow y = \frac{1}{2} w_{m,x} \sqrt{1 - \left(\frac{z}{\frac{1}{2}h}\right)^2}$$

$$\text{because } w_{z,x} = w_{m,x} \sqrt{1 - 4\left(\frac{z}{h}\right)^2} \quad (6)$$

Begin Derivation of Pressure Gradient

$$\frac{dp}{dx} = - \left(\frac{64}{N \text{Re}'} \right)^{\frac{1}{2}} \mathbf{r} V^2 \frac{1}{D_H}$$

Insert equation 3

$$\frac{dp}{dx} = - \left(\frac{(64)^{\frac{1}{2}} \mathbf{r} (V_{x,z})^2 K' 8^{n'-1} \left(0.75 + \frac{1}{4n'} \right)^{n'}}{\mathbf{r} (V_{x,z})^{2-n'} D^{n'+1}} \right) \quad (\text{z direction}) \quad (7)$$

$$\frac{dp}{dx} = - \left(\frac{\left(32 (V_{x,z})^{n'} K' 8^{n'-1} \left(0.75 + \frac{1}{4n'} \right)^{n'} \right)}{(2w_{z,x})^{n'+1}} \right)$$

$$\text{or } (V_{x,z})^{n'} = - \frac{\frac{dp}{dx} (2w_{z,x})^{n'+1}}{32 K' 8^{n'-1} \left(0.75 + \frac{1}{4n'} \right)^{n'}}$$

$$\therefore (V_{x,z}) = - \left(\frac{\frac{dp}{dx}}{K' 2^{5+3(n'-1)}} \right)^{\frac{1}{n'}} \frac{(2w_{z,x})^{1+\frac{1}{n'}}}{\left(0.75 + \frac{1}{4n'} \right)} \quad (8)$$

Applying the continuity equation

$$q_i = \int_{-\frac{1}{2}h}^{\frac{1}{2}h} V_{x,z} dA_x = 2 \int_0^{\frac{1}{2}h} V_{x,z} w_{z,x} dz$$

Insert $V_{x,z}$ from equation 8 and $w_{z,x}$ from equation 6

$$q_i = -2 \left(\frac{dp}{K' 2^{5+3(n'-1)} dx} \right)^{\frac{1}{n'}} \frac{2^{1+\frac{1}{n'}}}{\left(0.75 + \frac{1}{4n'}\right)} \int_0^{\frac{1}{2}h} (w_{m,x})^{2+\frac{1}{n'}} \left(1 - \left(\frac{2z}{h}\right)^2\right)^{\frac{2+\frac{1}{n'}}{2}} dz$$

$$q_i = - \left(\frac{dp}{K' 2^{2+3n'}} \right)^{\frac{1}{n'}} \frac{(2w_{m,x})^{2+\frac{1}{n'}}}{\left(0.75 + \frac{1}{4n'}\right)} \int_0^{\frac{1}{2}h} \left(1 - \left(\frac{2z}{h}\right)^2\right)^{1+\frac{1}{2n'}} dz$$

Let $u = 2z / h$

Set $t = [1 - (u)^2]^{1/2}$

Then $dz = \frac{h}{2} du$

At $z = 0 \Rightarrow u = 0$

At $z = h / 2 \Rightarrow u = 1$

The limits of the integral become: $u = 0 \Rightarrow t = 1$, $u = 1 \Rightarrow t = 0$

Separately evaluating the following integral

$$\int_0^1 t^{(2+\frac{1}{n'})} du$$

For power law fluid, $n' < 1$ for example $n' = 0.89$ in which case $2+1/n' = 2 + 1/0.89 = 3.12$

The solution is known from the table of integrals

$$\int t ds = \frac{5}{2}t + \frac{1}{2} \sin^{-1} s$$

$$\int t^3 ds = \frac{1}{4}st^3 + \frac{3}{8}st + \frac{3}{8} \sin^{-1} s$$

$$\int t^5 ds = \frac{1}{6}st^5 + \frac{5}{24}st^3 + \frac{5}{16}st + \frac{5}{16} \sin^{-1} s$$

The power that t is raised to in the integral is between the limits $5 \geq (2 + 1/n') \geq 3$.

The solution to the integral is known for the two limits of t^3 and t^5 .

$$\int_0^1 t^3 du = \frac{ut^3}{4} + \frac{3ut}{8} + \frac{3}{8} \sin^{-1} u$$

$$\int_0^1 t^5 du = \frac{ut^5}{6} + \frac{5ut^3}{24} + \frac{5ut}{16} + \frac{5}{16} \sin^{-1} u$$

Therefore, after integration and evaluation of the limits from $0 \rightarrow 1$, all of the $u \cdot t$ products are zero. The only term left is the $\sin^{-1}(u)$ term which is $\pi / 2$.

$$\therefore \int_0^1 t^3 du = \frac{6}{32} p \quad \text{and} \quad \int_0^1 t^5 du = \frac{5}{32} p$$

The integral of interest lies between these two values. Using linear interpolation this value can be found.

$$\int_0^1 t^{(2+\frac{1}{n'})} du = \frac{p}{32} \left[6 - \left(\frac{(2+\frac{1}{n'})-3}{5-3} \right) \right] = \frac{p}{32} \left[6 - \frac{1}{2} \left(\frac{1}{n'} - 1 \right) \right] = \frac{p}{64} \left[13 - \frac{1}{n'} \right]$$

For $n' = 0.89$ the error in assuming $n' = 1$ is

$$\frac{13 - \frac{1}{0.89}}{13 - 1} = \frac{11.87}{12} = 0.99 \text{ or } 1\% \text{ Thus it is ignored.}$$

$$\therefore q_i = - \left(\frac{\frac{dp}{dx}}{K' 2^{2+3n'}} \right)^{\frac{1}{n'}} \frac{(2w_{m,x})^{2+\frac{1}{n'}}}{\left(0.75 + \frac{1}{4n'}\right)} \frac{hp}{128} \left[13 - \frac{1}{n'} \right] \quad (9)$$

Solve for $-dp/dx$

$$-\frac{dp}{dx} = \frac{q_i^{n'} K' 2^{2+3n'} \left(0.75 + \frac{1}{4n'}\right)^{n'} 128^{n'}}{(2w_{m,x})^{2n'+1} (hp)^{n'} \left[13 - \frac{1}{n'} \right]^{n'}} \quad (10)$$

Next consider how p and $w_{m,x}$ vary along length of fracture by differentiating.

$$w_{m,x} = (p - \sigma_{\min}) / (E' / 2h) \quad (11)$$

$$\text{or } \frac{dp}{dx} = \frac{E'}{2h} \frac{dw_{m,x}}{dx} \quad (12)$$

Insert dp/dx from equation 10

$$-\frac{dp}{dx} = \frac{q_i^{n'} K' 2^{2+3n'} \left(0.75 + \frac{1}{4n'}\right)^{n'} 128^{n'}}{(2w_{m,x})^{2n'+1} (h\mathbf{p})^{n'} \left[13 - \frac{1}{n'}\right]^{n'}} = \frac{E'}{2h} \frac{dw_{m,x}}{dx}$$

Separate variables and integrate

$$\therefore \frac{q_i^{n'} K' 2^{2+3n'} \left(0.75 + \frac{1}{4n'}\right)^{n'} 128^{n'}}{2^{2n'+1} (h\mathbf{p})^{n'} \left[13 - \frac{1}{n'}\right]^{n'}} \int_x^{L_f} dx = \frac{E'}{2h} \int_{w_{m,x}}^0 (w_{m,x})^{2n'+1} dw_{m,x}$$

$$\therefore \frac{q_i^{n'} K' 2^{2+3n'} \left(0.75 + \frac{1}{4n'}\right)^{n'} 128^{n'}}{2^{2n'+1} (h\mathbf{p})^{n'} \left[13 - \frac{1}{n'}\right]^{n'}} (L_f - x) = \frac{E' (w_{m,x})^{2n'+2}}{2h(2n'+2)}$$

$$w_{m,x} = \left(\frac{q_i^{n'} K' 2^{2+3n'} \left(0.75 + \frac{1}{4n'}\right)^{n'} 128^{n'}}{2^{2n'+1} (h\mathbf{p})^{n'} \left[13 - \frac{1}{n'}\right]^{n'}} \frac{2h(2n'+2)}{E'} (L_f - x) \right)^{\frac{1}{2n'+2}}$$

$$\text{For simplicity } B = \left(\frac{K' 2^{2+3n'} \left(0.75 + \frac{1}{4n'}\right)^{n'} 128^{n'}}{2^{2n'+1} (h\mathbf{p})^{n'} \left[13 - \frac{1}{n'}\right]^{n'}} \frac{2h(2n'+2)}{E'} \right)^{\frac{1}{2n'+2}}$$

if $x = 0$ then $w_{m,x} = w_{m,0}$

$$\therefore w_{m,x} = BQ^{\frac{n'}{2n'+2}} (L_f - x)^{\frac{1}{2n'+2}} \quad (13)$$

$$\text{and } w_{m,0} = Bq_i^{\frac{n'}{2n'+2}} (L_f)^{\frac{1}{2n'+2}} = \frac{2h\Delta p}{E'} \quad (14)$$

$$L_f = f(q_i, w_{m,o}) \Rightarrow L_f = \left(\frac{w_{m,o}}{Bq_i^{\frac{n'}{2n'+2}}} \right)^{2n'+2}$$

Conclusion: If the pumping rate, q_i , doubles then L_f reduces to $\frac{1}{2^{\frac{n'}{2n'+2}}}$ for example

when $n' = 0.89$ L_f reduces to 83%.

With the width known, one can integrate the fracture volume, Vol_f , by using the

average width. $w_{av} = \frac{p}{4} w_{m,x}$ or $A_x = \frac{hp}{4} w_{m,x}$

$$Vol_f = \int_0^{L_f} A_x dx = \frac{hp}{4} \int_0^{L_f} w_{m,x} dx \quad \therefore w_{m,x} = Bq_i^{\frac{n'}{2n'+2}} (L_f - x)^{\frac{1}{2n'+2}}$$

$$Vol_f = \frac{Bq_i^{\frac{n'}{2n'+2}} hp}{4} \int_0^{L_f} (L_f - x)^{\frac{1}{2n'+2}} dx$$

$$Vol_f = \frac{Bq_i^{\frac{n'}{2n'+2}} hp}{4} \left(\frac{(L_f)^{\frac{2n'+3}{2n'+2}} (2n'+2)}{2n'+3} \right) \quad (15)$$

$$L_f = f(Vol_f, q_i) = \left(\frac{4Vol_f (2n'+3)}{Bq_i^{\frac{n'}{2n'+2}} hp (2n'+2)} \right)^{\frac{2n'+2}{2n'+3}}$$

Another important measurable parameter is the friction pressure loss

Inside the fracture, $\Delta p = p_{w,o} - \sigma_{min}$. Rewriting equation 14 yields

$$\Delta p = \frac{E' w_{m,0}}{2h} \Rightarrow \Delta p = \frac{E'}{2h} Bq_i^{\frac{n'}{2n'+2}} (L_f)^{\frac{1}{2n'+2}}$$

The volume equation and the Δp equation both have the term q_i in common.

$$\frac{\Delta p 2h}{E' (L_f)^{\frac{1}{2n'+2}}} = Bq_i^{\frac{n'}{2n'+2}} = \frac{4Vol_f (2n'+3)}{hp (2n'+2) (L_f)^{\frac{2n'+3}{2n'+2}}}$$

Solving gives

$$\Delta p = \frac{2E'Vol_f(2n'+3)}{h^2\mathbf{p}(2n'+2)L_f} \text{ which is } \Delta p = f(L_f, Vol_f)$$

or

$$L_f = \frac{2E'Vol_f(2n'+3)}{h^2\mathbf{p}(2n'+2)\Delta p} \text{ which is } L_f = f(\Delta p, Vol_f).$$

$$\Delta p = \frac{2E'Vol_f(2n'+3)}{h^2\mathbf{p}(2n'+2)\left(\frac{4Vol_f(2n'+3)}{Bq_i^{\frac{n'}{2n'+2}}h\mathbf{p}(2n'+2)}\right)^{\frac{2n'+2}{2n'+3}}}$$

$$\therefore \Delta p = (Vol_f)^{\frac{1}{2n'+3}} q_i^{\frac{n'}{2n'+2}} \left(\frac{E'(8n'+12)^{\frac{1}{2n'+3}} \mathbf{p} h B^{\frac{2n'+2}{2n'+3}}}{2\mathbf{p} h^2 (2n'+2)^{\frac{1}{2n'+3}}} \right)$$

The following derivation is also repeated for a Newtonian fluid.

The Reynolds number for a Newtonian fluid is given by

$$NRe = \frac{\mathbf{r}VD_H}{\mathbf{m}} \quad (16)$$

Derivation of Pressure Gradient for Newtonian Fluid

$$\frac{dp}{dx} = -\left(\frac{64}{NRe}\right)^{\frac{1}{2}} \mathbf{r}V^2 \frac{1}{D_H}$$

Insert equation 16

$$\frac{dp}{dx} = -\left(\frac{(64)^{\frac{1}{2}} \mathbf{r}(V_{x,z})^2 \mathbf{m}}{\mathbf{r}(V_{x,z})D_H^2}\right) \quad (\text{z direction}) \quad (17)$$

Insert equation 1 and simplify

$$\frac{dp}{dx} = - \left(\frac{(32V_{x,z} \mathbf{m})}{(2w_{z,x})^2} \right)$$

$$\text{or } (V_{x,z}) = - \frac{\frac{dp}{dx} (w_{z,x})^2}{8\mathbf{m}} \quad (18)$$

Applying the continuity equation

$$q_i = \int_{-\frac{1}{2}h}^{\frac{1}{2}h} V_{x,z} dA_x = 2 \int_0^{\frac{1}{2}h} V_{x,z} w_{z,x} dz$$

Insert $V_{x,z}$ from equation 18 and $w_{z,x}$ from equation 6

$$q_i = - \frac{\frac{dp}{dx} (w_{m,x})^3}{4\mathbf{m}} \int_0^{\frac{1}{2}h} \left(1 - \left(\frac{2z}{h} \right)^2 \right)^{\frac{3}{2}} dz$$

Let $u = 2z / h$

Then $dz = \frac{h}{2} du$

$$q_i = - \frac{\frac{dp}{dx} (w_{m,x})^3}{2h\mathbf{m}} \int (1 - u^2)^{\frac{3}{2}}$$

From a Table of Integrals

$$\int (a^2 - u^2)^{\frac{3}{2}} du = \frac{u}{8} (5a^2 - 2u^2) \sqrt{a^2 - u^2} + \frac{3a^4}{8} \sin^{-1} \frac{u}{a} + C$$

At $z = 0 \Rightarrow u = 0$

At $z = h / 2 \Rightarrow u = 1$

Thus you evaluate the integral explicitly.

Separately evaluating the following integral

$$\int_0^1 (a^2 - u^2)^{\frac{3}{2}} du = \frac{1}{8}(5-2)\sqrt{1-1} + \frac{3}{8} \sin^{-1} 1 - (0)$$

$$\therefore \int_0^1 (a^2 - u^2)^{\frac{3}{2}} du = \frac{3p}{8 \cdot 2} = \frac{3p}{16}$$

$$q_i = -\frac{\frac{dp}{dx} (w_{m,x})^3 h}{8m} \left(\frac{3p}{16} \right) \quad (19)$$

Solve for $-dp/dx$

$$-\frac{dp}{dx} = \frac{128q_i m}{(w_{m,x})^3 3hp} \quad (20)$$

Next consider how p and $w_{m,x}$ vary along length of fracture by differentiating.

$$w_{m,x} = (p - \sigma_{\min}) / (E' / 2h) \quad (22)$$

$$\text{or } \frac{dp}{dx} = \frac{E'}{2h} \frac{dw_{m,x}}{dx} \quad (23)$$

Insert dp/dx from equation 20

$$-\frac{dp}{dx} = \frac{128q_i m}{(w_{m,x})^3 3hp} = \frac{E'}{2h} \frac{dw_{m,x}}{dx}$$

Separate variables and integrate

$$\therefore -\frac{256q_i m}{3pE'} \int_x^{L_f} dx = \int_{w_{m,x}}^0 w_{m,x}^3 dw_{m,x}$$

$$\therefore \frac{256q_i m}{3pE'} (L_f - x) = \frac{1}{4} w_{m,x}^4$$

$$w_{m,x} = \sqrt[4]{\frac{1024q_i m}{3pE'} (L_f - x)} \quad (24)$$

if $x = 0$ then $w_{m,x} = w_{m,0}$

$$\text{and } w_{m,o} = \sqrt[4]{\frac{1024q_i \mathbf{m}}{3pE'}} (L_f) = \frac{2h\Delta p}{E'} \quad (25)$$

$$L_f = f(q_i, w_{m,o}) \Rightarrow L_f = \left(\frac{w_{m,o}^4 3pE'}{1024q_i \mathbf{m}} \right)$$

With the width known, one can integrate the fracture volume, Vol_f , by using the

$$\text{average width. } w_{\text{av}} = \frac{p}{4} w_{m,x} \text{ or } A_x = \frac{hp}{4} w_{m,x}$$

$$\text{Vol}_f = \int_0^{L_f} A_x dx = \frac{hp}{4} \int_0^{L_f} w_{m,x} dx$$

$$\text{Vol}_f = \frac{hp}{4} \left(\frac{1024q_i \mathbf{m}}{3pE'} \right)^{\frac{1}{4}} \int_0^{L_f} (L_f - x)^{\frac{1}{4}} dx$$

$$\text{Let } u = (L_f - x) \text{ and } du = -dx$$

$$\text{Then } \int -u^{\frac{1}{4}} dx = -\frac{4}{5} u^{\frac{5}{4}} = -\frac{4}{5} (L_f - x)^{\frac{5}{4}} \Big|_0^{L_f}$$

$$\text{Vol}_f = \frac{hp}{5} \left(\frac{1024q_i \mathbf{m}}{3pE'} \right)^{\frac{1}{4}} L_f^{\frac{5}{4}} \quad (26)$$

$$L_f = f(\text{Vol}_f, q_i) = \left(\frac{5\text{Vol}_f}{hp} \right)^{\frac{4}{5}} \left(\frac{3pE'}{1024q_i \mathbf{m}} \right)^{\frac{1}{5}}$$

Another important measurable parameter is the friction pressure loss

Inside the fracture, $\Delta p = p_{w,o} - \sigma_{\text{min}}$. Rewriting equation 24 yields

$$\Delta p = \frac{E' w_{m,0}}{2h} \Rightarrow \Delta p = \frac{E'}{2h} \left(\frac{1024q_i \mathbf{m}}{3pE'} \right)^{\frac{1}{4}} (L_f)^{\frac{1}{4}}$$

The volume equation and the Δp equation both have the term q_i in common.

$$\left(\frac{1024q_i \mathbf{m}}{3pE'} \right)^{\frac{1}{4}} = \frac{5\text{Vol}_f}{hpL_f^{\frac{5}{4}}} = \frac{2h\Delta p}{E' L_f^{\frac{1}{4}}}$$

Solving gives

$$L_f = \frac{5Vol_f E'}{2ph^2 \Delta p} \text{ which is } L_f = f(\Delta p, Vol_f).$$

If q_i is constant and Fluid Efficiency is constant then Vol_f is the only variable.

$Vol_f \sim \text{time (t)}$.

$$\frac{\log(p)}{\log(\Delta t)} \approx \frac{1}{2n'+3} \cong \frac{1}{5}$$

Both Δp and Vol_f can be measured during fracturing at constant q_i . Δp increases in bottom hole pressure and assuming two equal and opposite fractures, then compute

$Vol_f = \text{Vol pumped} * \text{Fluid Efficiency}$.

Another relation can be derived such as such as $\Delta p = f(q_i, Vol_f)$ by eliminating L_f from these two equations.

$$L_f = \frac{\left(\frac{5Vol_f}{ph}\right)^{\frac{4}{5}}}{\left(\frac{1024mq_i}{3pE'}\right)^{\frac{1}{5}}} = \frac{\left(\frac{2h\Delta p}{E'}\right)^4}{\left(\frac{1024mq_i}{3pE'}\right)}$$

$$\text{Solving for } \left(\frac{2h\Delta p}{E'}\right)^4 = \left[\left(\frac{5Vol_f}{ph}\right)\left(\frac{1024mq_i}{3pE'}\right)\right]^{\frac{4}{5}}$$

$$\therefore \Delta p = \left(\frac{E'}{2h}\right)\left(\frac{5120Vol_f m}{3p^2 h E'}\right)^{\frac{1}{5}} q_i^{\frac{1}{5}}$$

Toward the end of the job, when the specified volume has been pumped or Vol_f is known, it can be concluded that if the flow rate had been doubled then Δp would have been $2^5 = 32$ times as high.

While pumping at a constant q_i , the volume pumped and thus the fracture volume, Vol_f , grow linearly in time.

APPENDIX B

```
'Ron Pack
'File: case4.BAS

'A = Tube Area
'Af = Fracture Area
'B1,B2 = Impedance
'BM,BP = Constants During Time Step In Compatibility
Equations
'c = Wave Propagation Velocity (ft/sec)
'CdAp = Perforation Area
'CM,CP = Constants During Time Step In Compatibility
Equations
'D = Inside Tube Diameter (in)
'delt = Time Step (sec)
'dff = Pressure loss across fracture (psf)
'dft = Pressure loss across tubing (psf)
'dffx = Pressure loss per section of fracture (psf)
'dftx = Pressure loss per section of tubing (psf)
'delH = dftx in feet of head
'delhf = dff in feet of head
'delperf = Pressure loss across perforations (psf)
'Dh = Fracture Hydraulic Diameter
'fD = Lord/McGowan Friction factor
'G = Gel G (lb/Mgal)
'h = Fracture height (ft)
'Hf = Fracture head
'Ht = Tube head
'K = K' for fluid
'Lf = Fracture Length (ft)
'Lt = Tube Length (ft)
'n = n' for Gel
'N1 = Number of Tube Stations
'N2 = Number of fracture stations
'P = Proppant Concentration (lb/gal)
'Pin = In-Situ Stress
'Q = Steady State Flow rate
'Qf = Fracture Flowrate
'Qt = Tube Flow rate
'R1,R2 = Resistance Coefficient
'rho = Fluid Density
'TMAX = Program Running Time
'V = Tube Velocity
'Vf = Velocity inside fracture
'Vol = Volume pumped into fractures
'w = Fracture Width
```

```

CLS

OPEN "a:output.dat" FOR OUTPUT AS #1
Lt = 8000
D = 2.441
Q = 14
rho = 1.946
n = .789
K = .000614
c = 4000
Delt = .1
CdAp = .013897
N1 = 20
G = 20
P = 0
Lf = 800
Vol = 788
mu = .0000179 `water
h = 70
N2 = 2
Pin = 6400
TMAX = 30
NS1 = N1 + 1
NS2 = N2 + 1

DIM Qt(NS1), Ht(NS1)
DIM Qf(NS2), Hf(NS2)

'Initial steady state tube calculations
Pi = 4 * ATN(1)
A = (Pi / 4) * (D / 12) ^ 2
Q1 = Q * .09359
V = Q1 / A
delx = c * Delt
tau = 4 * Lt / c

'Lord/McGowan Friction Factor calculation for the tubing
NRe = (1.934 * V * (D / 12)) / mu
fD = (4 * .046) / (NRe ^ .2)
sig = .207492288#
fD1 = fD * sig
R1 = (fD1 * delx) / (2 * 32.2 * (D / 12) * (A ^ 2))
B1 = c / (32.2 * A)
CV = ((CdAp) ^ 2) * 32.2

```

```

'Friction loss across tubing and perforations
calculations
dft = (.5 * fD1 * (rho) * V ^ 2 * (Lt / (D / 12)))
dftx = dft / N1
delH = dftx / (32.2 * rho)
delperf = (.5 * rho * ((Q1 / CdAp) ^ 2))

'Initial steady state fracture calculations
VolFrac = Vol / 2
w = VolFrac / (h * Lf)
Dh = 2 * w
Af = w * h
Q2 = Q1 / 2
Vf = Q2 / Af

'Friction coefficient calculation for the fracture
NRef = (rho * Vf ^ (2 - n) * Dh ^ n) / (K * 8 ^ (n - 1)
* ((3 * n + 1) / (4 * n)) ^ n)
fDf = 64 / NRef
R2 = (fDf * delx) / (2 * 32.2 * Dh * (Af ^ 2))
B2 = c / (32.2 * Af)
P1 = Pin * 144
Hin = P1 / (rho * 32.2)

'Pressure loss calculation across fracture
dff = .5 * fDf * rho * Vf ^ 2 * (Lf / Dh)
dffx = dff / N2
delhf = dffx / (rho * 32.2)
P11 = P1 + dff + delperf + dft
h11 = P11 / (32.2 * rho)
T = 0

'Steady state calculations
FOR I = 1 TO NS1
Qt(I) = Q1
IF I = 1 THEN Ht(I) = h11 ELSE Ht(I) = h11 - delH
PRINT #1, USING "#####.#####"; T; Qt(I); Ht(I)
h11 = Ht(I)
NEXT I
h21 = Ht(NS1) - (delperf / (32.2 * rho))

FOR I = 1 TO NS2
Qf(I) = Q2
IF I = 1 THEN Hf(I) = h21 ELSE Hf(I) = h21 - delhf
PRINT #1, USING "#####.#####"; T; Qf(I); Hf(I)
h21 = Hf(I)

```

```

NEXT I

'Transient calculations
KMAX = INT(.5 * TMAX / Delt) + 1
FOR K = 1 TO (KMAX - 1)
T = 2! * Delt * K

'Tubing interior points
FOR I1 = 2 TO 3
    FOR I = I1 TO N1 STEP 2
        CP1 = Ht(I - 1) + (Qt(I - 1) * B1)
        CM1 = Ht(I + 1) - (Qt(I + 1) * B1)
        BP1 = B1 + (R1 * ABS(Qt(I - 1)))
        BM1 = B1 + (R1 * ABS(Qt(I + 1)))
        Ht(I) = (CP1 * BM1 + CM1 * BP1) / (BP1 + BM1)
        Qt(I) = (Ht(I) - CM1) / BM1

'Tube inlet boundary condition
        CM11 = Ht(2) - (B1 * Qt(2))
        BM11 = B1 + (R1 * ABS(Qt(2)))
        IF T < (tau / 2) THEN Qt(1) = Q1 - (.65513 / 2) *
(1 - COS(Pi * (T / (.5 * tau)))) ELSE Qt(1) = Q1 - .65513
        Ht(1) = (Qt(1) * BM11) + CM11
        NEXT I
NEXT I1

'Fracture interior positions
FOR I2 = 2 TO 3
    FOR I = I2 TO N2 STEP 2
        CP2 = Hf(I - 1) + Qf(I - 1) * B2
        CM2 = Hf(I + 1) - Qf(I + 1) * B2
        BP2 = B2 + R2 * ABS(Qf(I - 1))
        BM2 = B2 + R2 * ABS(Qf(I + 1))
        Hf(I) = (CP2 * BM2 + CM2 * BP2) / (BP2 + BM2)
        Qf(I) = (Hf(I) - CM2) / BM2

'Tube exit boundary condition
        CM21 = Hf(2) - (Qf(2) * B2)
        BM21 = B2 + (R2 * ABS(Qf(2)))
        CP1NS = Ht(N1) + Qt(N1) * B1
        BP1NS = B1 + (R1 * ABS(Qt(N1)))
        Qt(NS1) = (-CV * (BP1NS + (BM21 / 2))) + SQR((CV
^ 2) * (BP1NS + (BM21 / 2)) ^ 2 + (2 * CV * (CP1NS -
CM21)))
        Ht(NS1) = CP1NS - (BP1NS * Qt(NS1))

'Fracture inlet boundary condition

```

```

      Qf(1) = Qt(NS1) / 2
      Hf(1) = CM21 + (BM21 * Qf(1))

'Fracture exit boundary condition
      CP2NS = Hf(N2) + Qf(N2) * B2
      BP2NS = B2 + (R2 * ABS(Qf(N2)))
      Hf(NS2) = P1 / (rho * 32.2)
      Qf(NS2) = (CP2NS - Hf(NS2)) / BP2NS
      NEXT I
NEXT I2

'Variable storage
FOR I = 1 TO NS1
PRINT #1, USING "#####.#####"; I; T; Qt(I); Ht(I)
NEXT I
FOR I = 1 TO NS2
PRINT #1, USING "#####.#####"; I; T; Qf(I); Hf(I)
NEXT I
NEXT K
END

```

VITA

Name: Stephen Ronald Pack, Jr.

Date of Birth: December 1, 1973

Place of Birth: Beckley, West Virginia

Education: Master of Science in Mechanical Engineering
West Virginia University, Morgantown, WV
December, 1998

Bachelor of Science in Mathematics and
Teacher Certification for Grades 7-12
Liberty University, Lynchburg, VA
May, 1996

Hinton High School, Hinton, WV
June, 1992

VELOCITY PROFILE IN CONFINED ELLIPTIC FRACTURES

By

Stephen Ronald Pack, Jr.

A Thesis

Submitted to
West Virginia University
In Partial Fulfillment of the Requirements
For the Degree of
Master of Science

APPROVAL OF EXAMINING COMMITTEE

Kenneth Means, Ph.D.

Scott Wayne, Ph.D.

Date

John Loth, Ph.D., Chair